Combining Raloxifene and Mechanical Loading Improves Bone Composition and Mechanical Properties in a Murine Model of Chronic Kidney Disease (CKD)

[1,2,3] Rachel K. Surowiec, PhD; [3] Olivia N. Reul; [3] Nusaiba N. Chowdhury, MS; [4] Ratan K. Rai, PhD; [3] Dyann Segvich; [3] Andrew A. Tomaschke, PhD; [1] John Damrath, PhD; [3] Andrea M. Jacobson; [5,6] Matthew R. Allen, PhD; [3]Joseph M. Wallace, PhD

[1] Weldon School of Biomedical Engineering, Purdue University, West Lafayette, IN; [2] Department of Radiology and Imaging Sciences, Indiana University School of Medicine, Indianapolis, IN; [3] Department of Biomedical Engineering, Indiana University Purdue University Indianapolis, Indianapolis, IN; [4] Department of Biochemistry and Molecular Biology, Indiana University School of Medicine, Indianapolis, IN; [5] Department of Anatomy, Cell Biology, and Physiology, Indiana University School of Medicine, Indianapolis, IN; [6] Roudebush Veterans Administration Medical Center, Indianapolis, IN

- Matthew R. Allen, PhD, matallen@iu.edu
- Nusaiba N. Chowdhury, MS, nnchowdh@iu.edu
- John Damrath, PhD, jdamrath@iu.edu
- Andrea M. Jacobson, jacoband@iu.edu
- Ratan K. Rai, PhD, rkrai@iu.edu
- Olivia N. Reul, oreul@iu.edu
- Dyann Segvich, dsegvich@iu.edu
- Rachel K. Surowiec, PhD; rsurowie@purdue.edu
- Andrew A. Tomaschke, PhD, atomasch@iu.edu
- Joseph M. Wallace, PhD, jmwalla@iupui.edu

Corresponding Author:

Rachel K. Surowiec, PhD
Assistant Professor, Weldon School of Biomedical Engineering (primary)
Assistant Professor, Radiology and Imaging Sciences (adjunct)
Purdue University
723 W. Michigan St. SL 220N
Indianapolis, IN 46202
317.278.3506 rsurowie@purdue.edu

Abstract

Introduction

Patients with chronic kidney disease (CKD) are at an alarming risk of fracture compared to age and sex-matched non-CKD individuals. Clinical and preclinical data highlight two key factors in CKD-induced skeletal fragility: cortical porosity and reduced matrix-level properties including bone hydration. Thus, strategies are needed to address these concerns to improve mechanical properties and ultimately lower fracture risk in CKD. We sought to evaluate the singular and combined effects of mechanical and pharmacological interventions on modulating porosity, bone hydration, and mechanical properties in CKD.

Methods

Sixteen-week-old male C57BL/6J mice underwent a 10-week CKD induction period via a 0.2% adenine-laced casein-based diet (n=48) or remained as non-CKD littermate controls (Con, n=48). Following disease induction (26 weeks of age), n=7 CKD and n=7 Con were sacrificed (baseline cohort) to confirm a steady-state CKD state was achieved prior to the initiation of treatment. At 27 weeks of age, all remaining mice underwent right tibial loading to a maximum tensile strain of 2050 με 3x a week for five weeks with the contralateral limb as a non-loaded control. Half of the mice (equal number CKD and Con) received subcutaneous injections of 0.5 mg/kg raloxifene (RAL) 5x a week, and the other half remained untreated (UN). Mice were sacrificed at 31 weeks of age. Serum biochemistries were performed, and bi-lateral tibiae were assessed for microarchitecture, whole bone and tissue level mechanical properties, and composition including bone hydration.

Results

Regardless of intervention, BUN and PTH were higher in CKD animals throughout the study. In CKD, the combined effects of loading and RAL were quantified as lower cortical porosity and improved mechanical, material, and compositional properties, including higher matrix-bound water. Loading was generally responsible for positive impacts in cortical geometry and structural mechanical properties, while RAL treatment improved some trabecular outcomes and material-level mechanical properties and was responsible for improvements in several compositional parameters. While control animals responded positively to loading, their bones were less impacted by the RAL treatment, showing no deformation, toughness, or bound water improvements which were all evident in CKD. Serum PTH levels were negatively correlated with matrix-bound water.

Discussion

An effective treatment program to improve fracture risk in CKD ideally focuses on the cortical bone and considers both cortical porosity and matrix properties. Loading-induced bone formation and mechanical improvements were observed across groups, and in the CKD cohort, this included lower cortical porosity. This study highlights that RAL treatment superimposed on active bone formation may be ideal for reducing skeletal complications in CKD by forming new bone with enhanced matrix properties.

Key Words: Bone hydration; material properties; mechanical properties; chronic kidney disease; cortical porosity; Raloxifene

Introduction

Individuals with chronic kidney disease (CKD) have up to a 17-fold higher risk of fragility fracture than aged-matched non-CKD populations, leading to morbidity, a downward spiral in quality of life, and elevated mortality [1, 2]. There is rigorous scientific evidence that CKD predominantly affects cortical bone – in contrast to osteoporosis, which is typically associated with trabecular bone loss[3, 4]. The cortical bone phenotype in CKD occurs primarily in the formation/expansion of cortical pores (holes within the cortex). Clinical and preclinical data highlight that cortical porosity is correlated with compromised bone mechanical properties and fracture[5]. While methods to prevent new cortical pore formation have been well studied [6], less is known about approaches to infill existing cortical pores and the mechanical implications of this pathological pore infilling on fracture mechanics. We have demonstrated that cortical pores are dynamic [7], and infilling through active bone formation can be stimulated preclinically through PTH suppression in an animal model of CKD[8]. It is well accepted that mechanical loading is a potent anabolic stimulus for bone[9, 10]. In the context of CKD, Avin et al. demonstrated that exercise had multiple beneficial systemic effects in a rat model, including reduced cortical porosity, suggesting repetitive loading may be a non-pharmaceutical technique to minimize porosity [11]. Even though resolving cortical porosity in CKD is essential, improving porosity alone is likely not enough to mitigate mechanical deficits.

We[12] and others[13] have described impaired bone matrix properties in CKD which are also linked to bone brittleness, including modifications in collagen cross-linking and alterations in matrix-bound water. These tissue-level alterations can significantly and independently affect whole bone fracture resistance[14, 15]. Bound water decreases with age resulting in compromised mechanical and estimated material-level properties, including toughness [16]. Conversely, higher water within the Haversian canals and pathological pores (free water) is indicative of stiffer and more porous tissue[17]. Our laboratory has shown that animals with CKD have reduced matrix-bound water, and this reduction is associated with reduced mechanical properties [12, 18]. Accordingly, increasing matrix-bound water may be a promising therapeutic option for improving fracture resistance in CKD.

Raloxifene, an FDA-approved selective estrogen receptor modulator, has been shown to increase bound water at the collagen-mineral interface in a non-bone cell and non-estrogen mediated manner[19, 20]. We have shown that non-viable CKD bone exposed to raloxifene had higher bound water and improved toughness and post-yield mechanical properties compared to vehicle control [18]. When administered in vivo, raloxifene can increase bound water under non-CKD conditions [21 22]. In rats with polycystic progressive CKD, raloxifene beneficially impacted tissue-level and whole bone mechanical properties, and CKD animals given raloxifene had significantly lower cortical porosity compared to the untreated CKD animals. However, hydration, neither bound or free/pore water was not a measured outcome, and whether raloxifene can modulate water when administered under CKD conditions in vivo remains unknown [23]. Together, results support further exploration of raloxifene on matrix-bound water and tissue-level mechanical properties under CKD conditions.

Together, treatment to enhance matrix-bound water during a bone-building regime that targets cortical porosity infilling may be an ideal scenario for reducing skeletal complications in CKD by forming new bone with enhanced matrix properties. As such, we sought to determine the singular and combined effects of mechanical and pharmacological interventions on pore infilling, matrix hydration, and mechanical properties in CKD. We hypothesized that mechanical stimuli would initiate cortical porosity infilling, and raloxifene would improve the hydration of new bone through increased matrix-bound water

and together, would improve mechanical and material level outcomes. Key outcomes included cortical porosity, matrix hydration, tissue composition, and whole bone and regional mechanical properties.

Materials and Methods

2.1. Animals and Study Design

All animal procedures received Institutional Animal Care and Use Committee approval from the Science Animal Resource Center through the Indiana University Purdue University Indianapolis School of Science prior to initiating studies. Fifteen-week-old male C57BL/6J mice (B6; JAX #000664; n = 96) were ordered from Jackson Laboratories (Bar Harbor, ME, USA). Animals were housed three to five per cage at an institutionally approved animal facility with 12-hour light/dark cycles, an average temperature of 70° F, and access to food and water ad libitum. At 16 weeks of age, half of the mice were given an 0.2% adenine-laced casein-based diet (0.9% phosphorous, 0.6% calcium) to induce CKD (n=48 CKD). The remaining control littermates (n=48) were given the purified casein-based diet (0.9% phosphorous, 0.6% calcium) (Envigo Teklad Diets, Madison, WI, USA). After six weeks on the adenine-laced chow, the CKD cohort was switched to the control casein-based diet for four weeks as previously described to complete the CKD induction [24]. Mice were monitored daily during CKD induction, and body weights were measured weekly throughout the course of the study. Following induction (26 weeks of age), a subset of animals (n=7 CKD and n=7 control) were euthanized as the baseline cohort to confirm a steady CKD disease state was reached at the time of treatment initiation.

An additional five mice per group (n=5 CKD, n=5 control) were utilized in a strain calibration study to determine the average force necessary to induce a tensile strain of 2050 microstrain (με) on the tibia's anteromedial surface during compressive loading [9]. With the sacrificed mouse intact, an incision was made on the right tibiae, strain gauges were placed on the antero-medial surface proximal to the point of tibia and fibular articulation using cyanoacrylate glue followed by a polyurethane coating. Tibia were loaded using a mechanical testing machine and a 45 N load cell. The tibiae were loaded using a 4 Hz haversine waveform while the load was increased in 1 N increments from 1-15 N. The strain values recorded for each animal at various load levels were averaged within their respective groups. Strain was plotted as a function of load, and a linear regression analysis was conducted to determine the force necessary in each group to produce a strain of 2050 με.

Starting at 26 weeks of age, half of the remaining CKD and control mice received subcutaneous injections of 0.5 mg/kg raloxifene hydrochloride (RAL, Sigma-Aldrich, R1402) in a 10% 2-hydroxypropyl-β-cyclodextrin (Sigma-Aldrich, 332607) solution five times a week for five weeks (n=18 CKD RAL, n=18 control RAL). The remaining CKD and control mice remained untreated (UN; n=18 CKD UN, n=18 control UN). All mice (n=72) underwent *in vivo* axial compressive cyclic loading three times a week for five weeks using a Bose ElectroForce 3220 test instrument. Mice were anesthetized with 2% isoflurane and the right tibia underwent compressive cyclic loading, which consisted of 2 cycles at 4 Hz to the determined maximum load from the strain calibration study detailed above, followed by 1 second rest at 2N, repeated 110 times for a total of 220 compressive cycles per loading day and 3,300 compressive cycles throughout the study. The contralateral tibia (left) served as an internal non-loaded control. All mice received intraperitoneal injections of the fluorochrome calcein (30 mg/kg body mass) on days 3 and 33 relative to the start of loading/treatment to delineate areas of new bone formation during the five-week intervention.

At 31 weeks of age (following five weeks of treatment and loading), animals were anesthetized via vaporized inhaled isoflurane and euthanized via cardiac exsanguination followed by cervical dislocation. Blood was collected and serum was isolated and stored at -20° for serum biochemistries.

Kidneys were removed, weighed, fixed in 10% neutral buffered formalin for 24 hours, and stored in 70% ethanol. Bi-lateral tibiae were wrapped in phosphate buffered saline (PBS)-soaked gauze and stored at -20° C until analysis. A detailed graphical overview of the study can be found in **Figure 1**.

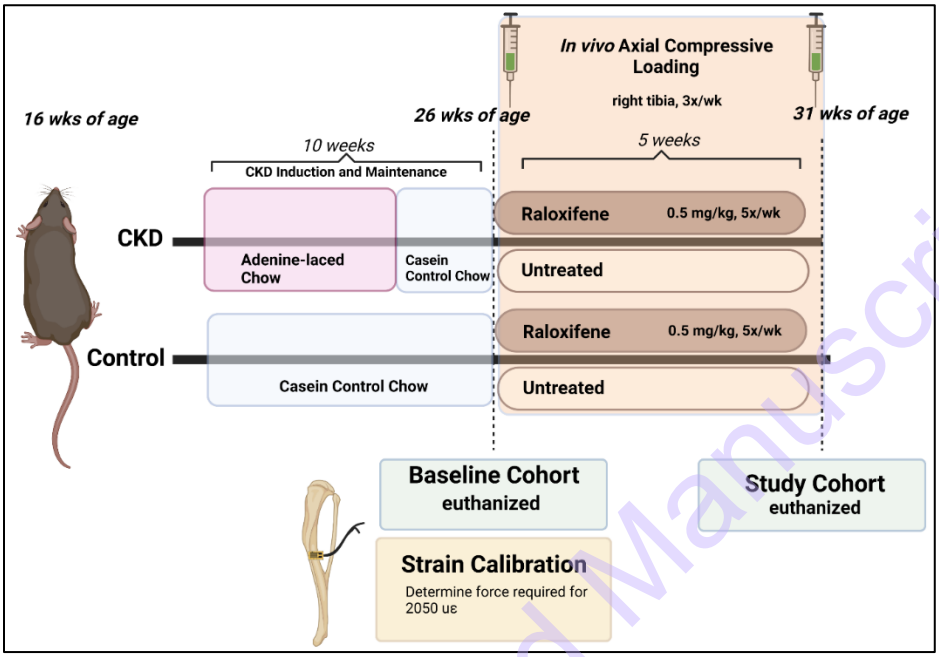

Figure 1. Detailed Study Schematic. Beginning at 16 wks of age, male C57BL/6 mice were randomly assigned to the chronic kidney disease (CKD) cohort which underwent a 10-week CKD induction and maintenance protocol or remained as non-CKD controls. At 26 weeks of age, the baseline cohort was euthanized, and an additional pilot cohort was euthanized to determine the optimal load necessary to induce 2050 με of strain on the tibia during cyclic axial compressive loading. All mice underwent in vivo axial compressive loading of the right tibia 3x week for 5 weeks. Half the mice in each group (CKD, Control) received 0.5 mg/kg of raloxifene 5x week for 5 weeks. Calcein fluorochrome injections were given at the start and end of treatment to denote bone formed during the intervention period. Mice were euthanized at 31 wks of age for analyses detailed in the methods section.

2.2. Serum Biochemistries

Blood collected at euthanasia was used to measure serum blood urea nitrogen (BUN) via colorimetric assay to assess the presence of kidney disease (BioAssay Systems, Hayward, CA, USA). Serum 1–84 parathyroid hormone (PTH) was measured via ELISA (Immnotopics Quidel, San Diego, CA, USA).

2.3. Microcomputed Tomography (μCT) and Analysis

Bi-lateral tibiae were scanned while hydrated using a nominal isotropic voxel size of 7.9 μm through a 0.5 mm aluminum filter (V= 59 kV, *I* = 167 μA) with a 0.7-degree angle increment and two frames averaged (SkyScan 1172, Bruker, Billerica, MA, USA). Two manufacturer-supplied cylindrical hydroxyapatite phantoms (0.25 and 0.75 g/cm^3 Ca-HA) were scanned daily using the same parameters. Scans were reconstructed (NRecon, Bruker), rotated to the same orientation (DataViewer, Bruker), and calibrated (CTAn, Bruker) to the hydroxyapatite-mimicking phantoms prior to analysis. Following scanning, tibiae were immediately wrapped in PBS-soaked gauze and stored at -20°C until further testing.

A 1 mm trabecular region of interest (ROI) was selected, beginning at the distal end of the proximal growth plate and extended distally. Trabecular bone was automatically segmented from the cortex and analyzed for bone volume fraction (BV/TV), trabecular thickness (Tb.Th), number (Tb.N), separation (Tb.Sp), and tissue mineral density (TMD) using CT Analyzer (CTAn, Bruker). Intracortical analysis was conducted using a 0.1 mm ROI at 20% of the bone's total length (proximal to distal) to capture a region with high cortical porosity that is just proximal to the maximum tensile strain region (located at 37% of the bone's total length). The cortical bone was automatically segmented by first applying a global threshold with a lower grey threshold: upper grey threshold of 70:255 followed by an ROI shrink wrap which stretched over holes on the surface of 4 pixels in diameter, and analyzed for cortical thickness (Ct.Th), total area (T.Ar), cortical area (Ct.Ar), marrow area (Ma.Ar), bone area fraction (BA/TA), and bone mineral density (BMD). Cortical porosity (Ct.Po) was calculated as the void area between the periosteal and endosteal surfaces and presented as a percentage of the overall cortical volume.

2.4. Four-point Bending Test to Failure

Bi-lateral tibiae from 12 mice per group (control UN, control RAL, CKD UN, CKD RAL) were randomly selected to undergo four-point bends test to failure with the medial surface in tension with lower support span at 9 mm and upper loading span at 3 mm (TA Instruments ElectroForce 3200). Tibiae samples were thawed immediately prior to testing, hydration was maintained throughout the test with PBS, and bones were loaded at a displacement control rate of 0.025 mm/s. Cross-sectional cortical properties, described in detail above, were obtained from 10 transverse µCT slices at the failure location (location was measured using calipers). These cortical slices were used as cortical ROIs to be analyzed for geometric properties needed to convert the force displacement data into stress and strain (in order to estimate tissue level properties) using standard engineering equations [25]. To define the yield point, a line parallel to the linear portion of the stress strain curve but offset by 0.2% strain was computed and the position this line intercepted the stress-strain curve defined the yield point. Three left tibiae from control UN, one left tibia from CKD RAL, and one right tibia from CKD UN group were omitted from analysis due to rotation of the bone during the testing procedure, resulting in abnormal mechanical curves. In these cases, the contralateral limb was also removed from analysis.

2.5. Solid State Nuclear Magnetic Resonance (ssNMR) Spectroscopy with Magic Angle Spin (MAS)

Solid state nuclear magnetic resonance (ssNMR) spectroscopy was acquired on a subset of the loaded right tibiae (control UN=6, control RAL=5, CKD UN=7, CKD RAL=8) that had undergone four-point bending. ssNMR was utilized to quantify free and bound water fractions, inorganic material status, and structural changes associated with matrix collagen [26]. Tibiae were prepared by removing the proximal and distal ends, flushing marrow, and then finely cutting into solid cortical <1 mm^3 fragments and loaded into a 3.2 mm zirconium rotor with empty spaces covered with Teflon tape for stable spinning. All ssNMR spectra were recorded on a 400 MHz NMR spectrometer (Avance HD, Bruker Biospin, Switzerland) with a Bruker 3.2mm DVT probe. The magic angle spin (MAS) frequency was 10.0 kHz for all experiments. The MAS speed was controlled using Bruker's MAS pneumatic unit with an accuracy of ± 2 Hz.

A 1D one pulse ^{1}H NMR was recorded with 1k data points for a total acquisition time of 12 ms was used to measure total water[26]. Bound water was assessed by a 2D ^{1}H–^{31}P Heteronuclear Correlation (HetCor) experiment[26]. The total contact time was 1.0 ms and the maximum t_1 evolution time was 2.6 ms. The effective field during ^{1}H homonuclear decoupling period Phase Modulated Lee – Goldburg (PMLG) was 110 kHz and high power ^{1}H decoupling (100 kHz) was applied during t_2 period[27 28, 29]. A total of 32

transients per increment and a recycle delay of 4 seconds was utilized. The spectra were zero-filled, and sine bell apodization was used in both dimensions prior to Fourier transformation. Phosphorous (^{31}P) relaxation is an excellent tool to study bone inorganic components. ^{31}P T1 of inorganic apatite depends on structural OH-, which in turn influences mineral crystallinity[26, 30, 31]. To assess inorganic matrix integrity, we measured the T_1 relaxation of ^{31}P by utilizing an inversion recovery protocol with a relaxation delay of 1000 seconds. ^{13}C Cross Polarization (CP) spectra were recorded to assess structural changes associated with organic matrix content [32]. The CP spectra were recorded with a ramp cross polarization sequence, 1.0 ms contact time, and Small Phase Incremental Alteration (SPINAL-64) decoupling (100 kHz ^{1}H RF field) [28].

All spectra were processed using Bruker Topspin (V. 4.1.1., Bruker). All peaks were externally referenced to the spectra of water [26] or ratio of total water with respect to OH through peak integration[26] as previously described. The OH resonance was chosen as our internal reference because previous studies have demonstrated that the 1.4 ppm peak shows very little variance following dehydration of intact bone[33]. To determine the relative bound water content in relation to OH content from the HetCor experiments, a rectangular method of integration centered at the ^{1}H chemical shift at 0.4 ppm (OH) and 4.8 ppm (bound water) respectively. Finally, T_1 relaxation time of ^{31}P was calculated.

2.6. Colocalized Raman Spectroscopy and Dynamic Indentation Testing

Colocalized Raman spectroscopy (Renishaw inVia, Wotton-under-Edge, United Kingdom) and nano dynamic mechanical analysis (nanoDMA) (Bruker TI-980, Eden Prairie, MN, United States) were acquired using a custom hybrid system that allows for co-localization of measures. The right tibiae were prepared in a manner that maintained the hydrated state as previously described [34]. A 2 mm thick section was cut starting at 37% of the bone length, sanded, polished, and rinsed in deionized water to remove residual debris. Fluorescent imaging was performed (Leica EL6000, Leica Microsystems, Buffalo Grove, IL) with a Basler MED Ace camera (Basler AG, Arensburg, Germany) integrated into the Raman spectrophotometer to visualize regions of bone formed during treatment denoted by a double calcein label. Eight points were chosen within the calcein labeling to assess newly formed matrix, and eight intracortical points beyond the initial label were used to analyze pre-existing matrix (formed before the commencement of treatment), resulting in a total of 16 points per sample.

Spectra was acquired using a 785 nm laser. Eight accumulations were averaged at each point using a 10-second exposure at 50% laser power with a grating resolution of 1200 l/mm (633/780). Spectra were baseline corrected using an 11th-order polynomial, cosmic rays were removed, followed by smoothing with a modified Savitzky-Golay function. The following compositional parameters were calculated: type B carbonate substitution ($v1\text{-}CO_3^{2-}/v1\text{-}PO_4^{3-}$ band area), mineral crystallinity (inverse of the full width at half maximum of $v1\text{-}PO_4^{3-}$), mineral-to-matrix ratios for Amide I band ($v1\text{-}PO_4^{3-}$/Amide I band area), CH_2 wagging ($v1\text{-}PO_4^{3-}$/ CH_2 wagging intensity), and Amide III band ($v1\text{-}PO_4^{3-}$/Amide III band area). Parameters were averaged over 8 points per region yielding one value per parameter per region per specimen.

Indentation testing was performed using a $R_i = 1\mu m$ cono-spherical fluid cell probe. Samples were submerged in 1X PBS and remained submerged throughout indentation testing. Each indentation test used a constant strain rate CMX load function (TriboScan Software 10.2.0.12), oscillating the probe at 100 Hz and 5 µN dynamic load as the indenter was pushed into the material until a 1000 µN peak static load was achieved. The peak load was then held for 30 seconds before unloading. A lift segment was included at the start of each indentation test to ensure the probe was out of contact and the point of contact was

identified using the displacement at which load monotonically increased. Thermal drift was minimized during testing by including a 30-minute delay between test setup and indentation testing.

To assess the viscoelastic mechanical behavior as a function of indentation depth (*h*), a mean storage modulus (*E'*), loss modulus (*E"*) and tan delta (tan δ) were calculated for every 50 nm up to a depth of 200 nm, an indentation strain of 20% (h/R_i). E' is in phase with applied dynamic load and describes the material's elastic behavior, whereas E" is 90° out of phase and describes the material's viscous behavior. Tan δ, is the ratio of E' to E" and a measure of a material's ability to dissipate energy.

E' and E" are both calculated using:

$$E = \frac{k \times \sqrt{\pi}}{2 \times \sqrt{A_C}}$$

Where A_c is the indenter projected contact area, where k is the storage stiffness, k', when determining the storage modulus, or loss stiffness, k", when determining the loss modulus.

k' is calculated from the applied dynamic load and resulting dynamic displacement as:

$$k' = \frac{DynamicLoad \times \cos(\delta)}{DynamicDisplacement} + m_T \times \bar{\omega}^2 - k_T$$

Where δ is the phase lag between the dynamic load and dynamic displacement, m_t is the indentation transducer mass, $\bar{\omega}$ is the radial frequency, and k_T is the stiffness of the transducer.

k_{loss} is similarly calculated as:

$$k" = \bar{\omega} \times \left(\frac{DynamicLoad \times \sin(\delta)}{DynamicDisplacement \times \bar{\omega}} - C_s \right)$$

It is noted that the moduli here are reduced moduli, related to the sample moduli by:

$E_s' = (1 - \nu_s{}^2)\left(\frac{1}{E'} - \frac{1-\nu_i^2}{E_i}\right)^{-1}$ for the storage modulus, and

$E_s" = (1 - \nu_s{}^2)E"$ for the loss modulus

Where ν_s is the Poisson's Ratio of the sample, and ν_i and E_i are the Poisson's ratio and modulus of the indenter probe, respectively. The advantage of this approach is that there is no need to assume a Poisson's ratio for the material.

Indents were excluded from analysis if the dynamic displacement amplitude fell outside of the manufacturer recommended 1-3 nm, the load vs. displacement curve showed discontinuities, the static indentation load never achieved 700 μN, or if contact was never made with the sample.

Finally, indentation modulus was calculated from the unloaded portion of the load-indentation curve using the Oliver-Pharr method [35] which is better suited to capture viscoelastic rather than purely elastic response. Hardness (H) was calculated as the maximum load divided by the contact area of the indent.

2.7. Statistical Analysis

All statistical analyses were performed using GraphPad Prism (v.9), and significance was determined at $p \leq 0.05$. Data presented as mean +/- standard deviation unless otherwise denoted. Unpaired t-tests were utilized to determine differences between control and CKD in the baseline cohort for all outcomes. Body mass was analyzed via a 2x2 factorial ANOVA (disease-by-treatment) at week 1, week 6, week 10, and week 15 (endpoint) of the study. Endpoint serum biochemistries and kidney weights were analyzed via a 2x2 factorial ANOVA (disease-by-treatment). Cortical and trabecular μCT outcomes and whole bone mechanical testing outcomes of the bilateral tibiae were analyzed using repeated measures (RM) 2x2 factorial ANOVA (treatment-by-loading) within the disease state (control or CKD).

Only right tibiae were used for Raman, nanoindentation, and ssNMR. Raman and nanoindentation outcomes were assessed via a 2x2 factorial RM ANOVA (treatment-by-matrix age) within disease states (control or CKD) allowing us to evaluate whether RAL preferentially improved bone composition and tissue-level mechanical properties in newly formed bone vs. pre-existing bone. Total water, bound water, and ^{31}P T_1 relaxation by ssNMR were analyzed by a regular 2x2 factorial ANOVA (treatment-by-disease). Pearson correlation coefficients were used to evaluate presence of correlations between bound water vs. PTH and bound water vs. mechanical outcomes. Main and interaction effects are reported when the model ANOVA $p<0.05$ and significant interaction terms were followed by a Sidak post hoc analysis.

Results

Two UN adenine-fed mice died of unknown causes at week 10 and week 11; one UN control mouse died of unknown causes prior to the start of the study. This resulted in group sizes of baseline control (n=7), baseline CKD (n=7), UN control (n=17), RAL control (n=18), UN CKD (n=16), and RAL CKD (n=18).

Baseline Cohort

Baseline CKD mice had significantly lower body mass than control (CKD 22.86 ± 1.87 vs. control 30.17 ± 1.85 g, p<0.0001). Serum PTH I-84 and BUN were significantly higher in baseline CKD vs. control (both p<0.0001) (**Supplemental Fig. 1A**). Cortical bone geometry and microarchitecture and trabecular microarchitecture were significantly compromised with CKD (**Supplemental Table 1**). **Supplemental Fig. 1B-C**. shows significantly higher cortical porosity, significantly lower trabecular number, and impaired structural and tissue-level mechanical properties in CKD vs. control.

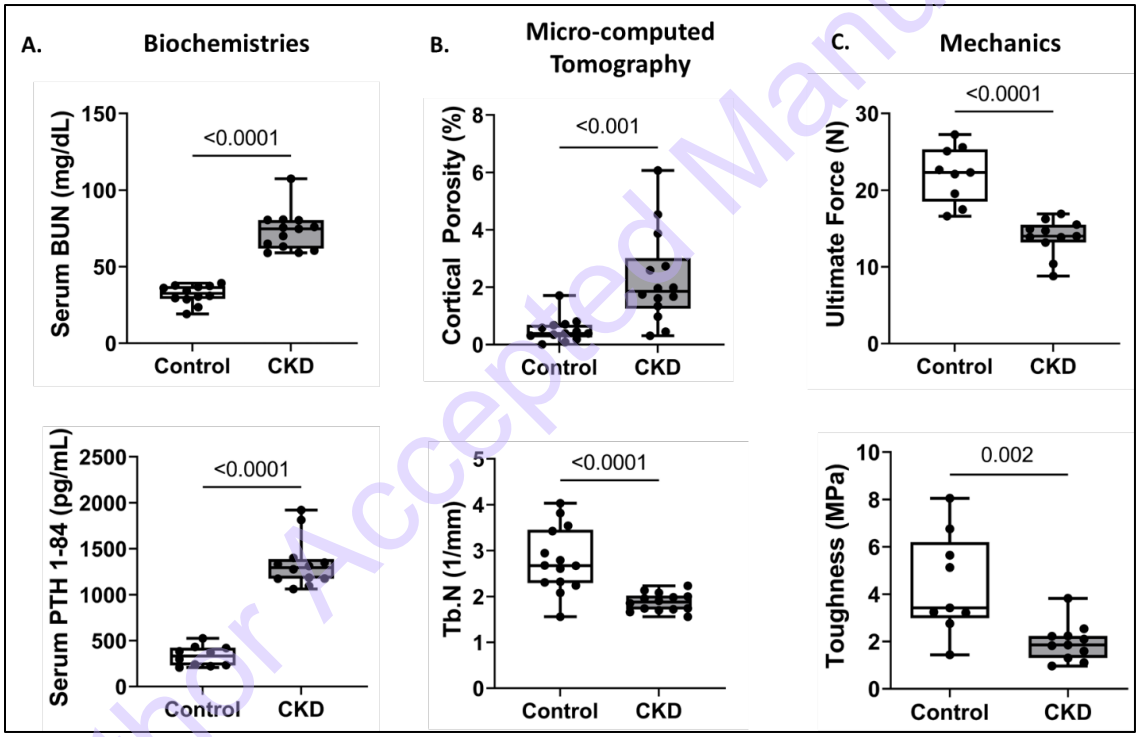

Supplementary Figure 1. Baseline cohort. N=7 CKD and control animals were sacrificed following the 10-week CKD induction period at 26 weeks of age to confirm a CKD disease state. A) Baseline CKD animals had significantly higher serum blood urea nitrogen (BUN) and serum parathyroid (PTH) levels compared to control littermates. B) Baseline CKD tibiae had significantly higher cortical porosity and altered cortical geometry and trabecular microarchitecture than baseline controls measured via micro-computed tomography (7.9 µm). C) Tibia from baseline CKD animals had lower ultimate force and toughness compared to baseline controls measured via four-point bending test to failure. Figure dipicts box and whisker plot; whiskers denote min. and max.

Supplementary Table 1. Trabecular and cortical properties of tibia (R) from baseline control and CKD mice via µCT.

	Baseline Control (Con)	Baseline Chronic Kidney Disease (CKD)	*p-value*
Trabecular Microarchitecture			
Bone volume fraction, BV/TV (%)	17.35 ± 2.4	8.72 ± 1.14	**<0.0001**
Trabecular thickness, Tb.Th (µm)	60.97 ± 4.86	46.55 ± 1.64	**<0.0001**
Trabecular spacing, Tb.Sp (µm)	200.2 ± 17.84	275.2 ± 13.4	**<0.0001**
Trabecular number, Tb.N (1/µm)	2.88 ± 0.57	1.87 ± 0.23	**0.001**
Tissue mineral density, TMD (g/cm^3)	0.76 ± 0.03	0.67 ± 0.01	**<0.0001**
Cortical Properties at 20% ROI			
Total area, T.Ar (mm^2)	1.85 ± 0.19	1.9 ± 0.08	0.61
Marrow area, Ma.Ar (mm^2)	0.92 ± 0.18	1.1 ± 0.1	**0.04**
Cortical area, Ct.Ar (mm^2)	0.93 ± 0.11	0.8 ± 0.04	**0.01**
Bone area fraction, BA/TA (%)	50.4 ± 5.84	42.05 ± 3.1	**0.007**
Cortical thickness, Ct.Th (mm)	0.15 ± 0.02	0.13 ± 0.02	**0.006**
Bone mineral density, BMD (g/cm^3)	1.13 ± 0.04	1.07 ± 0.03	**0.008**
Cortical porosity, Ct.Po (%)	1.34 ± 0.48	3.91 ± 1.46	**0.001**

Data provided as mean ± standard deviation. p-values from non-repeated measures t-tests are displayed and bolded when significance was reached at p≤0.05.

Body Mass

There were no differences in body mass of C57BL/6 mice prior to CKD induction. By week 6 of the induction, a significant main effect of disease ($p<0.0001$) was observed, with CKD mice having lower body mass vs. control (**Figure 2**). Following the resumption of the casein control diet, body mass in the CKD cohorts increased by 18% (CKD UN) and 7% (CKD RAL) but remained significantly lower than control mice (week 10, main effect of disease, $p<0.0001$). At study completion (week 15), there was a significant main effect of disease ($p<0.0001$) and treatment ($p<0.0001$) but no interaction ($p=0.75$). At this timepoint, CKD mice had lower body mass vs. control and mice treated with RAL had lower body mass than their UN counterparts within groups (CKD, control).

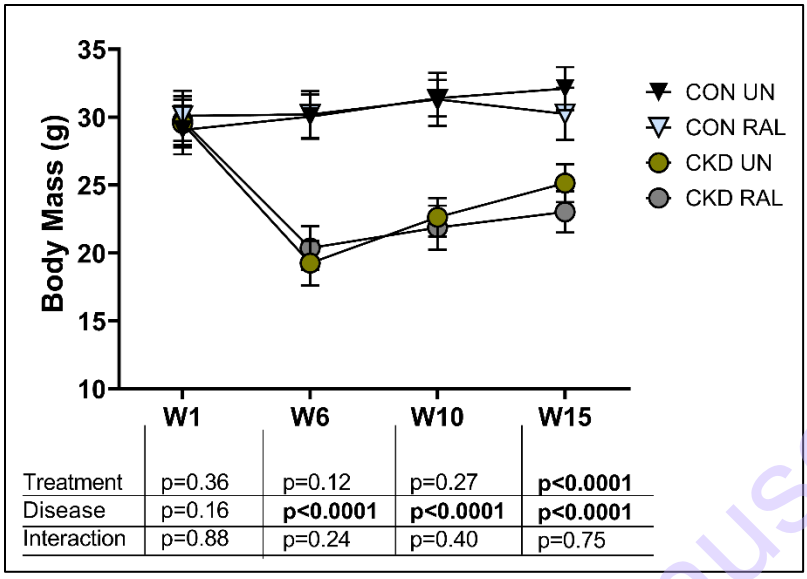

	W1	W6	W10	W15
Treatment	p=0.36	p=0.12	p=0.27	**p<0.0001**
Disease	p=0.16	**p<0.0001**	**p<0.0001**	**p<0.0001**
Interaction	p=0.88	p=0.24	p=0.40	p=0.75

Figure 2. Body mass. There were no significant differences in body mass among groups at the start of the study (week 1). At weeks 6 and 10, there was a significant main effect of disease where CKD animals had significantly reduced body mass due to CKD induction. By the study endpoint, we observed a significant main effect of disease and treatment where CKD animals had lower body mass and animals treated with raloxifene also had lower body mass vs. the untreated groups.

Biochemistries and indices of kidney disease

Two-way ANOVA results indicated a significant main effect of disease for serum BUN ($p<0.0001$) where all CKD mice had significantly higher levels, indicative of kidney disease, compared to control irrespective of treatment (**Fig.3A**). We observed a significant main effect of disease for serum PTH 1-84 ($p<0.0001$) with CKD mice having significantly higher levels (regardless of treatment) compared to the control cohort (**Fig.3B**). Kidney weight ratio (mg kidney weight/g body weight) demonstrated an interaction term ($p=0.01$) (**Fig.3C-D)**. Post-hoc analysis showed that CKD UN had lower kidney weights vs. control UN ($p=0.04$). Kidneys from animals treated with RAL had higher kidney weight ratios compared to their untreated counterparts regardless of disease (Control UN vs RAL: $p=0.02$; CKD UN vs RAL: $p<0.0001$).

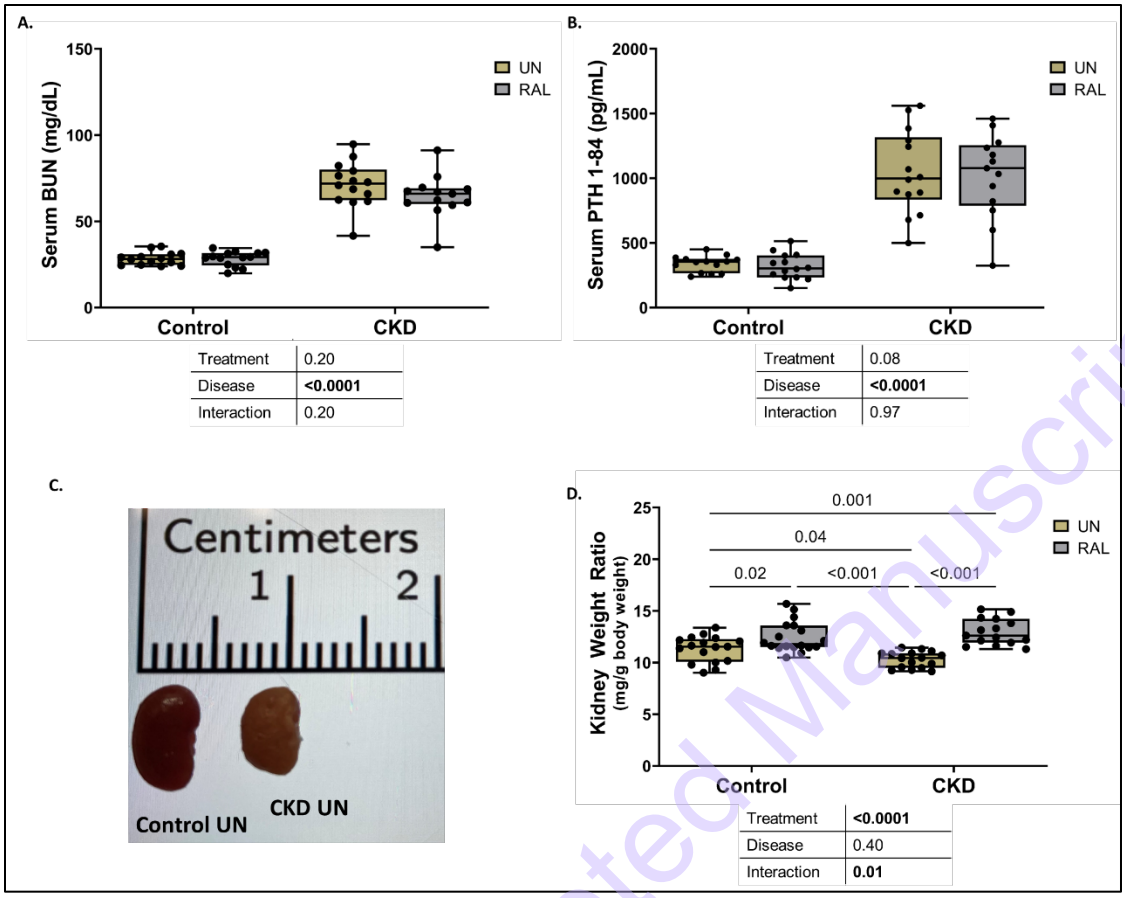

Figure 3. Serum biochemistries and indices of kidney disease. At the study endpoint, animals induced with CKD had significantly higher serum blood urea nitrogen (BUN, A) and higher serum parathyroid hormone 1-84 (PTH 1-84, B) compared to control. There was no significant difference in either serum biomarker due to raloxifene (RAL) treatment. C) Animals induced with CKD had kidneys that were smaller and discolored compared to controls. D) Analysis of kidney weight ratios demonstrated a significant effect of treatment and a significant interaction term. Post-hoc testing showed that RAL treatment significantly increased kidney weight ratio within the control cohort and the CKD cohort. Figure dipicts box and whisker plot; whiskers denote min. and max.

Cortical and trabecular bone geometry and microarchitecture

Detailed results from µCT analysis of cortical bone geometry and microarchitecture and trabecular microarchitecture, including RM two-way ANOVA results, can be found in **Table 1** and **Table 2**, respectively.

Control Cohort

Loading was more impactful than RAL treatment for cortical outcomes in the control cohort (**Table 1)**. However, a main effect of RAL treatment resulted in higher Ct.Ar ($p<0.0001$) and Ct.Po ($p=0.05$) irrespective of loading (**Figure 4A-B**). There were no significant interaction terms for any cortical outcome in the control cohort.

A main effect of loading was observed for Tb.N (p=0.02), and a main effect of treatment, loading, and interaction term was shown for BV/TV and Tb.Th (**Table 2**). Untreated loaded tibia had higher BV/TV and Tb.Th vs. UN non-loaded tibia and RAL non-loaded tibia had higher BV/TV and Tb.Th vs. UN non-loaded (**Table 2**).

CKD Cohort

Overall, the impact of loading and RAL was more robust in the CKD cohort. We observed a main effect of loading, which improved BA/TA (p=0.01) and Ct.Po (p<0.001). Loaded tibia had lower Ct.Po compared to the contralateral non-loaded tibia regardless of treatment (CKD UN non-loaded vs. loaded: 5.16 ± 2.66 vs. 3.27 ± 1.64%t; CKD RAL non-loaded vs. loaded: 5.97 ± 1.93 vs. 3.62 ± 1.76 %) (**Figure 4A-B**). Both loading and treatment significantly impacted Ct.Ar (p<0.0001 and p<0.01, respectively) and Ct.Th (p=0.01 and p<0.001, respectively); loaded RAL tibia had the highest Ct.Ar and Ct.Th compared to UN (**Table 1**). T.Ar had a significant interaction term (p<0.01). Post-hoc analysis showed non-loaded RAL tibia had higher T.Ar vs. non-loaded UN (p<0.01, 1.92 ± 0.14 vs. 1.78 ± 0.09, respectively) and loaded UN had higher T.Ar vs. non-loaded UN (p=0.01, 1.85 ± 0.001 vs. 1.78 ± 0.09, respectively). Post-hoc analysis following a significant interaction term for Ma.Ar (p=0.01) showed loaded RAL tibia had a smaller M.Ar vs. non-loaded RAL (**Table 1)**.

For the trabecular ROI, RAL improved BV/TV (p<0.001), Tb.Sp (p<0.0001), and Tb.N (p<0.0001). Loading improved Tb.Th (p=0.01) and TMD (p=0.01) (**Table 2**).

Table 1. Control and CKD cortical micro-computed tomography (μCT) outcomes.

Cortical Geometry and Microarchitecture	**Untreated (UN)**		**Raloxifene**		**Repeated Measures Two-Way Mixed Effects Model ANOVA**		
	Non-Loaded	**Loaded**	**Non-Loaded**	**Loaded**	Loading	Treatment	Loading x Treatment
CONTROL Cortical Properties at 20% ROI							
Total area, T.Ar (mm^2)	1.98± 0.15	2.06± 0.12	2.05± 0.16	2.08± 0.16	**<0.001**	0.41	0.07
Marrow area, Ma.Ar (mm^2)	0.97± 0.11	0.98± 0.09	0.99± 0.10	0.97± 0.11	0.70	0.83	0.09
Cortical area, Ct.Ar (mm^2)	1.02± 0.08	1.08± 0.05	1.06± 0.08	1.11± 0.08	0.15	**<0.0001**	0.54
Bone area fraction, BA/TA (%)	51.29± 2.89	52.47± 2.10	51.56± 2.20	53.50± 2.55	**<0.001**	0.38	0.33
Cortical thickness, Ct.Th (mm)	0.16± 0.01	0.17± 0.01	0.17± 0.01	0.18± 0.01	**<0.0001**	0.06	0.74
Cortical porosity, Ct.Po (%)	0.82± 0.90	0.62± 0.39	0.98± 0.50	1.07± 0.53	0.71	**0.05**	0.32
CKD Cortical Properties at 20% ROI							
Total area, T.Ar (mm^2)	1.78± 0.09 **$%**	1.85± 0.00**%**	1.92± 0.14 **$**	1.89± 0.12	0.30	**0.02**	**<0.01**
Marrow area, Ma.Ar (mm^2)	1.03± 0.10	1.05± 0.13	1.10± 0.12 **$**	1.04± 0.11 **$**	0.33	0.53	**0.01**
Cortical area, Ct.Ar (mm^2)	0.75± 0.05	0.79± 0.04	0.82± 0.05	0.85± 0.04	**<0.0001**	**<0.01**	0.57
Bone area fraction, BA/TA (%)	42.00± 3.46	43.20± 3.69	42.94± 2.65	45.11± 2.59	**0.01**	0.11	0.36
Cortical thickness, Ct.Th (mm)	0.12± 0.01	0.13± 0.01	0.13± 0.01	0.14± 0.01	**0.01**	**<0.001**	1.00
Cortical porosity, Ct.Po (%)	5.16± 2.66	3.27± 1.64	5.97± 1.93	3.62± 1.76	**<0.001**	0.24	0.65

Data provided as mean ± standard deviation. Repeated measures Two-way mixed effects ANOVA p-values are displayed and bolded when significant. Significant interactions were followed by post-hoc analyses and shared symbols indicate significant difference from one another.

Table 2. Control and CKD trabecular micro-computed tomography (µCT) outcomes.

Trabecular Microarchitecture	Untreated (UN)		Raloxifene		Repeated Measures Two-Way Mixed Effects Model ANOVA		
	Non-Loaded	Loaded	Non-Loaded	Loaded	Loading	Treatment	Loading x Treatment
CONTROL Trabecular Microarchitecture							
Bone volume fraction, BV/TV (%)	15.21± 3.33 **$&**	17.62± 2.96 **$**	18.65± 2.83 **&**	18.80± 2.05	**<0.0001**	**0.01**	**0.02**
Trabecular thickness, Tb.Th (µm)	59.78± 5.39 **$&**	66.27± 4.31 **$**	65.80± 0.65 **&**	68.53± 5.35	**<0.0001**	**0.02**	**0.03**
Trabecular spacing, Tb.Sp (µm)	220.39± 16.36	216.18± 13.90	214.49± 18.22	220.42± 16.71	0.38	0.62	0.09
Trabecular number, Tb.N (1/µm)	2.53± 0.48	2.66± 0.44	2.85± 0.50	2.75± 0.32	**0.02**	0.08	0.09
Tissue mineral density, TMD (g/cm^3)	0.77± 0.04	0.79± 0.03	0.78± 0.04	0.77± 0.03	0.19	0.51	0.07
CKD Trabecular Microarchitecture							
Bone volume fraction, BV/TV (%)	7.72± 1.04	7.85± 1.70	9.41± 1.17	9.46± 1.18	0.62	**<0.001**	1.00
Trabecular thickness, Tb.Th (µm)	52.17± 3.07	53.91± 4.41	51.03± 2.60	52.53± 3.39	**0.01**	0.25	0.90
Trabecular spacing, Tb.Sp (µm)	312.88± 19.12	311.03± 20.53	291.87± 16.04	291.67± 11.71	0.81	**<0.0001**	0.85
Trabecular number, Tb.N (1/µm)	1.48± 0.20	1.46± 0.30	1.85± 0.25	1.81± 0.23	0.49	**<0.0001**	0.91
Tissue mineral density, TMD (g/cm^3)	0.69± 0.02	0.71± 0.04	0.69± 0.03	0.70± 0.02	**0.01**	0.24	0.91

Data provided as mean ± standard deviation. Repeated measures Two-way mixed effects ANOVA p-values are displayed and bolded when significant. Significant interactions were followed by post-hoc analyses and shared symbols indicate significant difference from one another.

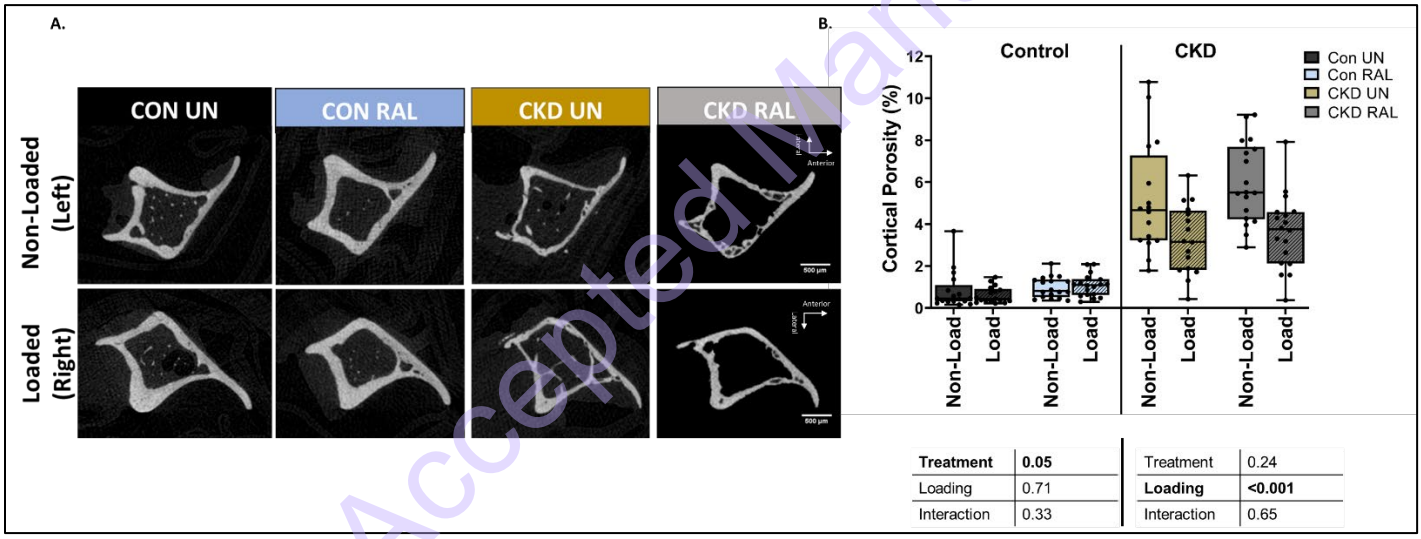

Figure 4. Cortical cross sections and cortical porosity. A) Representative microcomputed tomography (7.9 µm) cross-sectional images of bi-lateral tibia at 20% of the bone's total length from the proximal end in each group. This region was chosen for analysis because it captured an area with high cortical porosity in the CKD cohort and was located just proximal to the maximum tensile strain region (located at 37% of the bone's total length). B) For the CKD cohort, there was an effect of loading, which appeared to decrease porosity compared to the non-loaded tibia regardless of treatment. There was no significant impact of treatment on porosity in the CKD cohort. In the control animals, we observed an effect of treatment where RAL treated control tibia had higher cortical porosity than UN control, regardless of whether the limb was loaded or unloaded. Figure depicts box and whisker plot; whiskers denote min. and max. Con = control; UN = untreated; RAL= raloxifene, CKD = chronic kidney disease.

Whole bone and estimated tissue-level mechanical properties

Results from the four-point bending test to failure of control and CKD bi-lateral tibiae, including RM two-way ANOVA results, are detailed in **Table 3** and **Table 4**, respectively. Average force-displacement and stress-strain curves from the control and CKD tibiae can be found in **Supplementary Figure 2.**

Control Cohort

A main effect of loading was observed for the structural mechanical properties of ultimate force ($p<0.001$) and yield force ($p<0.0001$), which were both improved with loading. Work to yield had a significant interaction term ($p=0.04$). Post-hoc analysis showed loaded tibia had higher work to yield compared to non-loaded in UN controls. For estimated tissue-level properties, both loading and RAL significantly impacted yield stress ($p<0.001$ and $p=0.04$, respectively). Loading alone increased ultimate stress ($p<0.01$) regardless of treatment status. For resilience, the interaction term was significant ($p=0.04$). Post-hoc analysis showed that non-loaded UN and loaded RAL tibia had significantly lower resilience than loaded UN tibia (**Table 3)**.

CKD Cohort

Loading and RAL treatment were more impactful in CKD (**Supplementary Figure 2 and Table 4).** Loading improved ultimate force ($p<0.0001$), yield force ($p<0.01$), stiffness ($p=0.01$), work to yield ($p<0.01$), yield stress ($p=0.01$), ultimate stress ($p<0.01$), and resilience ($p=0.03$). RAL was responsible for improvements in post-yield displacement ($p=0.01$) and total strain ($p=0.01$). A significant main effect of loading and treatment was observed for total displacement ($p=0.09$ and $p=0.01$, respectively), post-yield work ($p=0.04$ and $p<0.01$, respectively), total work (both $p<0.01$), and toughness ($p<0.01$ and $p=0.01$), which was defined as the total area under the stress-strain curve.

Table3. Control four-point bending test structural and estimated tissue-level mechanical properties.

Control (CON)	**Untreated (UN)**		**Raloxifene**		**Repeated Measures Two-Way Mixed Effects Model ANOVA**		
	Non-Loaded	**Loaded**	**Non-Loaded**	**Loaded**	Loading	Treatment	Loading x Treatment
Structural mechanical properties from 4-point bending							
Ultimate force (N)	22.21 ± 5.12	26.72 ± 2.57	24.12 ± 2.79	26.40 ± 2.00	**<0.001**	0.44	0.20
Yield force (N)	21.09 ± 4.71	25.96 ± 2.52	21.66 ± 2.52	24.50 ± 2.33	**<0.0001**	0.68	0.20
Displ. to yield (µm)	212.24 ± 26.72	243.70 ± 53.05	216.93 ± 24.49	217.11 ± 21.94	0.12	0.28	0.13
Postyield displ. (µm)	72.67 ± 46.43	77.17 ± 131.60	97.25 ± 98.99	84.67 ± 54.15	0.89	0.58	0.74
Total displ. (µm)	284.90 ± 44.23	320.87 ± 142.03	314.18 ± 89.19	301.78 ± 51.79	0.67	0.87	0.38
Stiffness (N/mm)	113.43 ± 33.03	123.54 ± 33.19	113.01 ± 17.13	126.78 ± 12.02	0.07	0.81	0.86
Work to yield (mJ)	2.43 ± 0.54 **$**	3.39 ± 0.56 **$**	2.57 ± 0.45	2.91 ± 0.47	**<0.001**	0.28	**0.04**
Postyield work (mJ)	1.59 ± 1.18	1.84 ± 2.84	2.20 ± 2.16	2.13 ± 1.40	0.87	0.48	0.79
Total work (mJ)	4.01 ± 1.49	5.23 ± 2.77	4.77 ± 1.98	5.04 ± 1.24	0.22	0.63	0.44
Estimated tissue-level mechanical properties from 4-point bending							
Yield stress (MPa)	206.33 ± 36.77	255.70 ± 35.44	191.56 ± 43.75	213.96 ± 26.60	**<0.001**	**0.04**	0.12
Ultimate stress (MPa)	217.25 ± 39.25	262.60 ± 32.22	212.00 ± 41.99	230.17 ± 21.37	**<0.01**	0.13	0.12
Strain to yield (mε)	18.18 ± 2.19	20.59 ± 4.67	19.16 ± 2.25	19.18 ± 1.41	0.11	0.76	0.12
Total strain (mε)	24.51 ± 4.29	24.18 ± 6.49	28.11 ± 9.92	26.76 ± 4.79	0.58	0.20	0.86
Modulus (GPa)	12.82 ± 2.84	14.68 ± 5.43	11.44 ± 3.28	12.49 ± 1.53	0.10	0.18	0.59
Resilience (MPa)	2.05 ± 0.42 **$**	2.80 ± 0.49 **$&**	1.99 ± 0.45	2.25 ± 0.36 **&**	**<0.001**	**0.05**	**0.04**
Toughness (MPa)	3.39 ± 1.22	4.45 ± 2.92	3.65 ± 1.56	3.90 ± 0.99	0.25	0.80	0.48

Data provided as mean ± standard deviation. Repeated measures Two-way mixed effects ANOVA p-values are displayed and bolded when significant. Significant interactions were followed by post-hoc analyses and shared symbols indicate signifcant difference from one another.

Table 4. Chronic kidney disease (CKD) four-point bending test structural and estimated tissue-level mechanical properties.

Chronic Kidney Disease (CKD)	Untreated (UN)		Raloxifene		Repeated Measures Two-Way Mixed Effects Model ANOVA		
	Non-Loaded	Loaded	Non-Loaded	Loaded	Loading	Treatment	Loading x Treatment
Structural mechanical properties from 4-point bending							
Ultimate force (N)	14.09 ± 2.53	17.43 ± 3.29	15.40 ± 3.99	18.07 ± 3.53	**<0.0001**	0.44	0.57
Yield force (N)	12.35 ± 4.64	16.72 ± 3.55	13.78 ± 3.63	15.53 ± 3.99	**<0.01**	0.94	0.16
Displ. to yield (μm)	208.10 ± 64.49	217.31 ± 26.71	189.73 ± 22.34	206.00 ± 26.37	0.18	0.26	0.68
Postyield displ. (μm)	66.25 ± 91.60	50.08 ± 46.49	114.45 ± 118.94	232.00 ± 220.46	0.21	**0.01**	0.10
Total displ. (μm)	274.35 ± 88.35	267.39 ± 59.68	304.18 ± 101.55	442.68 ± 210.27	**0.09**	**0.01**	0.06
Stiffness (N/mm)	66.46 ± 16.64	86.00 ± 17.18	81.72 ± 18.19	85.23 ± 22.65	**0.01**	0.26	0.06
Work to yield (mJ)	1.50 ± 0.78	2.00 ± 0.53	1.44 ± 0.47	1.76 ± 0.50	**<0.01**	0.45	0.52
Postyield work (mJ)	0.76 ± 0.86	0.85 ± 0.79	1.55 ± 1.48	3.43 ± 2.52	**0.04**	**<0.01**	0.06
Total work (mJ)	2.26 ± 0.98	2.85 ± 1.01	3.00 ± 1.45	5.20 ± 2.44	**<0.01**	**<0.01**	0.07
Estimated tissue-level mechanical properties from 4-point bending							
Yield stress (MPa)	148.74 ± 58.13	201.05 ± 45.22	173.86 ± 52.55	185.20 ± 53.58	**0.01**	0.83	0.12
Ultimate stress (MPa)	169.53 ± 31.94	209.96 ± 44.84	191.58 ± 50.44	214.89 ± 48.78	**<0.01**	0.46	0.40
Strain to yield (mε)	18.67 ± 6.01	19.18 ± 2.63	17.48 ± 1.58	18.73 ± 2.80	0.38	0.48	0.70
Total strain (mε)	25.08 ± 9.68	23.53 ± 4.91	28.78 ± 11.69	39.77 ± 17.67	0.18	**0.01**	0.08
Modulus (GPa)	8.97 ± 2.37 $	11.80 ± 2.86 $	11.01 ± 2.50	11.06 ± 2.56	**0.03**	0.46	**0.04**
Resilience (MPa)	1.62 ± 0.85	2.12 ± 0.60	1.70 ± 0.66	1.93 ± 0.70	**0.03**	0.79	0.46
Toughness (MPa)	2.47 ± 1.15	3.04 ± 1.14	3.44 ± 1.65	5.55 ± 2.39	**<0.01**	**0.01**	0.05

Data provided as mean ± standard deviation. Repeated measures Two-way mixed effects ANOVA p-values are displayed and bolded when significant. Significant interactions were followed by post-hoc analyses and shared symbols indicate signifcant difference from one another.

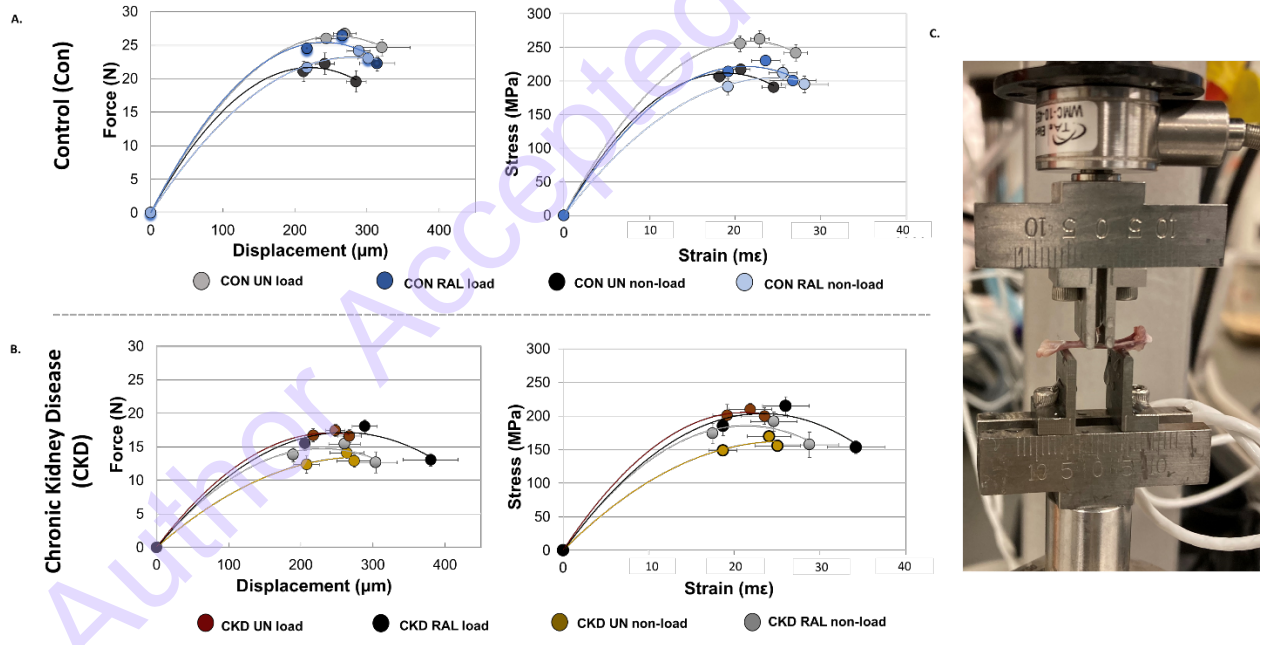

Supplemental Figure 2. Average force-displacement and average stress-strain plots from four-point bending mechanical testing of control (A) and chronic kidney disease (CKD) (B) bi-lateral tibia. Average force-displacement shows that CKD bones are weaker than control bones regardless of loading or RAL. For CKD, loaded bones had higher structural properties such as ultimate and yield force while RAL treated bones had improved post-yield displacement and total strain. For controls, loading also improved ultimate and yield force but RAL effects were much less pronounced. Data points in A and B are mean values ±

standard error of the mean and lines were created using a second-order polynomial function. UN = untreated; RAL = raloxifene. The four-point bending test setup is shown in C.

Solid State Nuclear Magnetic Resonance (ssNMR) spectroscopy

Total water was higher in controls vs. CKD, and treatment with RAL had higher total water vs. UN (main effect of disease $p<0.0001$ and treatment $p<0.0001$, **Fig.5A-B**). We observed a significant interaction term for bound water ($p=0.02$, **Fig.5C-D**). Control UN tibia had higher bound water vs. CKD UN. In the CKD cohort, treatment with RAL resulted in significantly higher bound water, bringing the mean to near control UN levels (**Fig.5C**). Further examination of bound water revealed a significant negative correlation with serum PTH levels, indicating that higher PTH levels were associated with lower bound water content ($r=-0.62$, $p=0.005$; **Fig. 5E**). Pearson's correlations revealed a significant positive relationship between bound water and post-yield displacement ($r=0.64$, $p=0.027$) and bound water and total strain (r0.64, $p=0.019$).

Regarding ^{31}P T_1, there was a significant main effect of disease ($p < 0.01$, **Fig. 5F**), with CKD animals exhibiting lower T_1 relaxation times compared to the control group. However, there was no significant impact of treatment. The natural abundance ^{13}C spectra of one CKD untreated and one CKD RAL spectra are shown in **Supplemental Figure 3**. Most of the resonances corresponded to Type 1 collagen residues. We did not observe a considerable difference between CKD and CKD-RAL. The carbonyl resonances still show 3 peaks, and the line width of aliphatic peaks did not show any considerable changes.

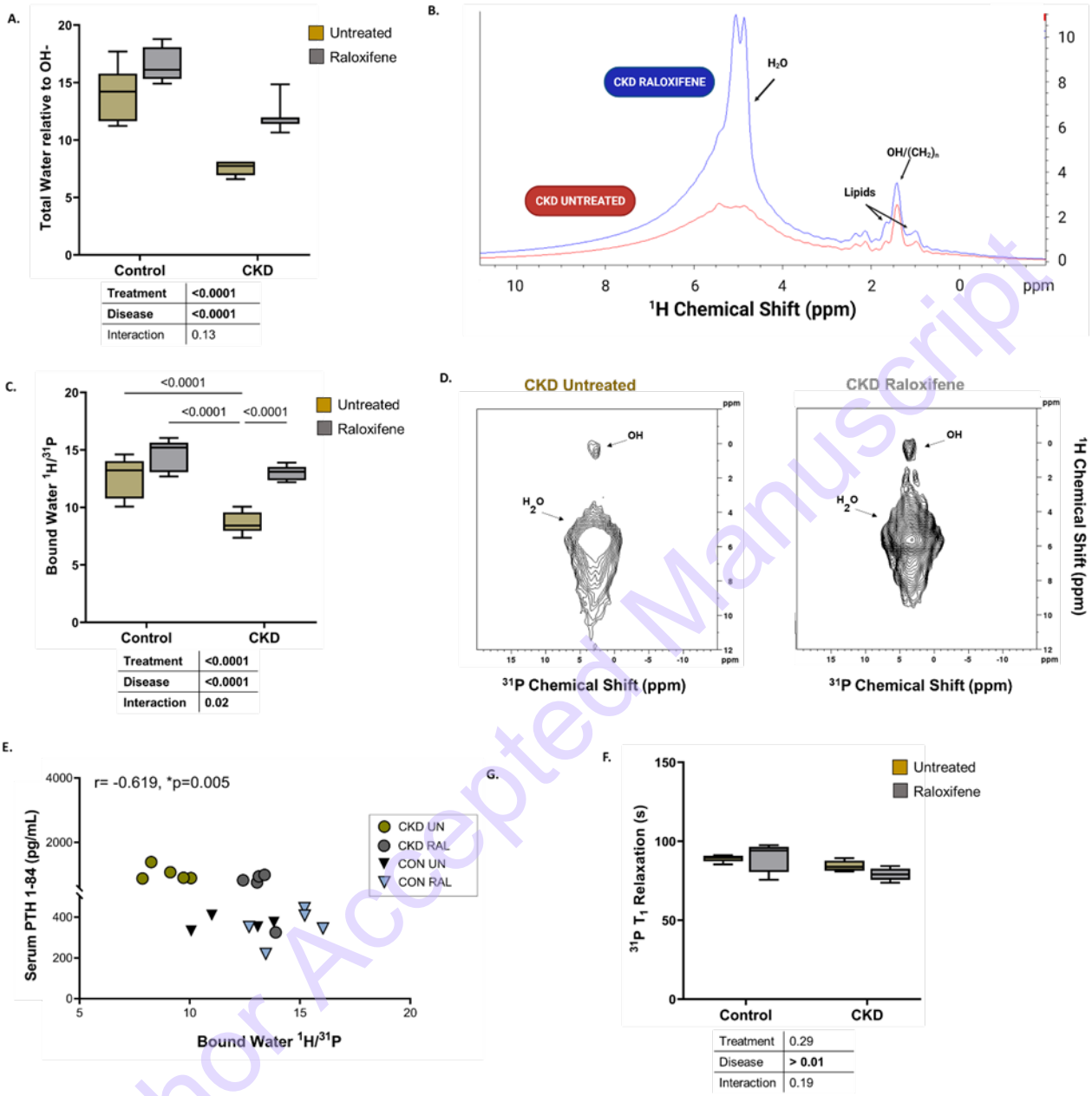

Figure 5. Solid-state nuclear magnetic resonance spectroscopy. A) Total water assessed by 1D one-pulse ^{1}H ssNMR revealed that control bone had higher total water than CKD, and treatment with raloxifene resulted in higher total water than untreated samples. B) Representative chemical shift spectra illustrated the elevated total water in CKD raloxifene-treated (blue) versus CKD untreated (red) samples. C) 2D HeTCor experiments for bound water determination showed that in CKD, raloxifene-treated animals had tibiae with higher bound water approaching control levels. D) Representative 2D HETCor spectra from one CKD untreated and one CKD raloxifene-treated sample, highlighting water and OH peaks. E) Serum parathyroid hormone (PTH) levels negatively correlated with bound water content measured by ssNMR. H) ^{31}P T_1 relaxation time revealed a significant main effect of disease but not treatment. A, C, and H dipict box and whisker plot; whiskers denote min. and max.

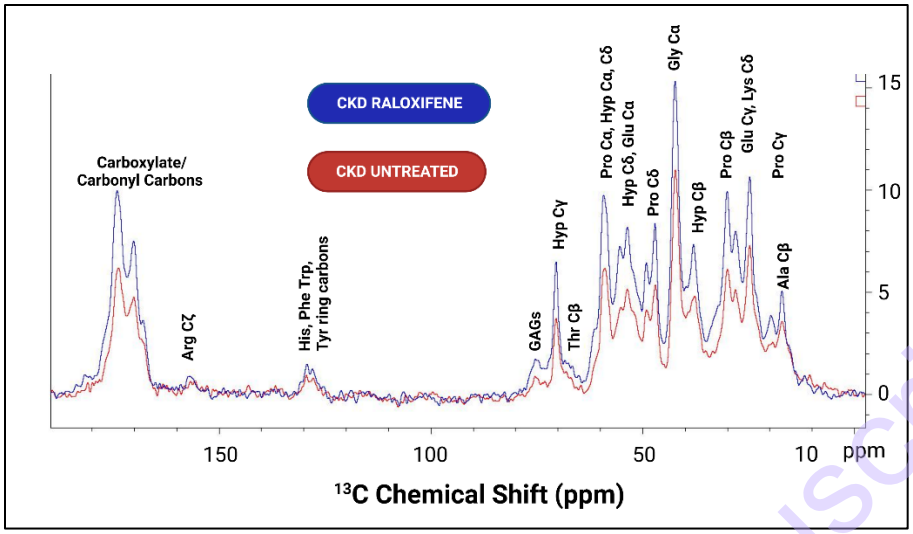

Supplemental Figure 3. Carbon 13 spectra from solid state nuclear magnetic resonance spectroscopy. A representative example ^{13}C chemical shift spectra from one CKD untreated (red) and one CKD raloxifene-treated tibia with peaks identified on the plot.

Co-localized Raman Spectroscopy and nanoindentation

Raman Spectroscopy

In CKD tibiae, we observed a significant interaction (p=0.02) for mineral crystallinity/maturity (**Fig.6A**). Raloxifene-treated pre-existing bone exhibited lower crystallinity than UN pre-existing bone (p=0.003), while new bone receiving RAL displayed higher crystallinity than pre-existing bone from RAL-treated animals (p<0.0001). A significant main effect of treatment emerged for relative mineralization using CH_2 wagging intensity (p=0.04, **Fig.6D**), with both pre-existing and new bone that had received RAL showing a lower mineral-to-matrix ratio compared to UN bone. In the control group, here was a significant main effect of matrix age for relative type B carbonate substitution (p=0.05, **Fig.6G**), with new bone displaying higher values than pre-existing bone. Raloxifene treatment resulted in a lower mineral-to-matrix ratio measuring CH_2 wagging (p=0.03, **Fig.6I**) and higher Amide III area (p=0.03, **Fig.6J**) compared to untreated samples.

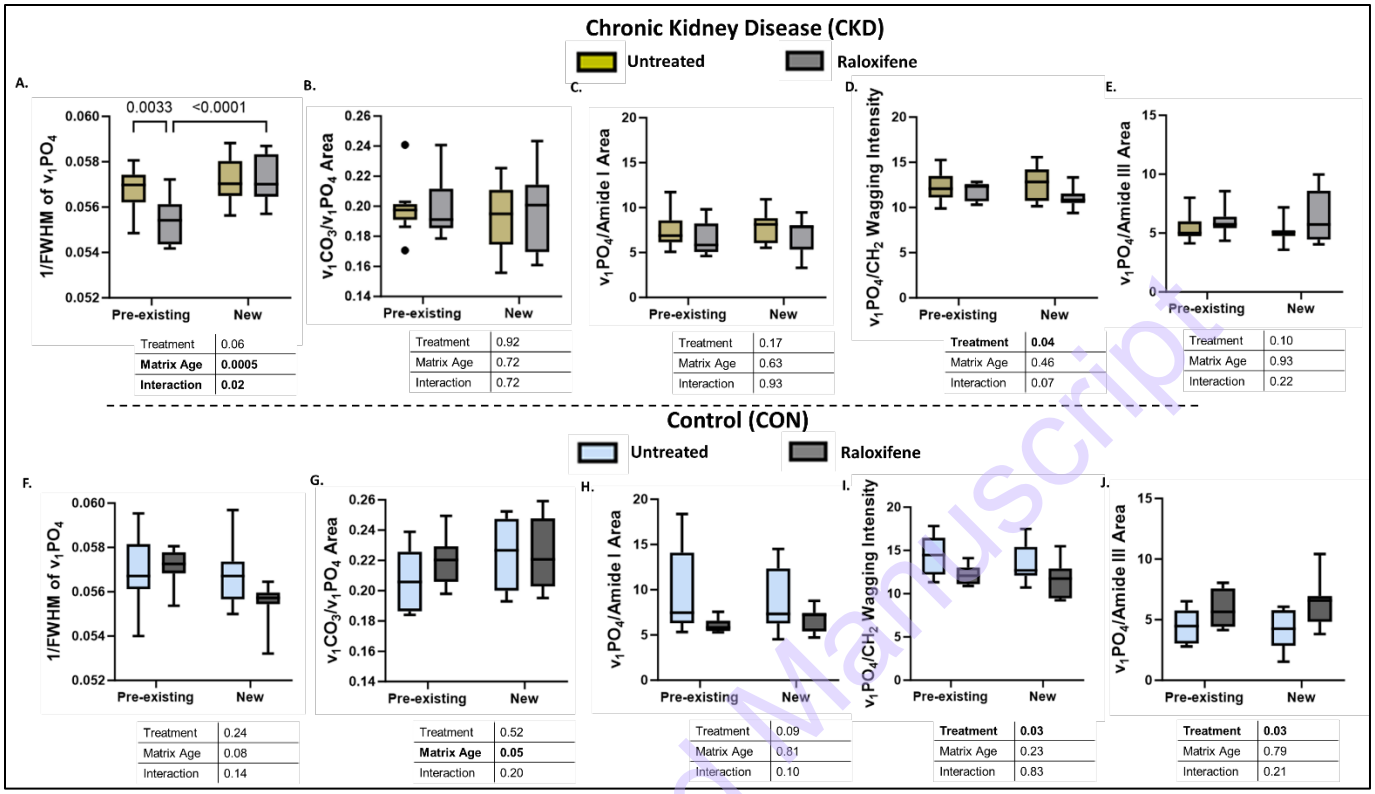

Figure 6. Raman Spectroscopy. A) For CKD, we noted a significant impact of matrix age and an interaction regarding mineral crystallinity/maturity. Raloxifene-treated pre-existing bone exhibited lower crystallinity than untreated pre-existing bone, and new bone receiving raloxifene displayed higher crystallinity than pre-existing bone from raloxifene-treated animals. No significant ANOVA terms were observed for relative type B carbonate substitution (B) or relative mineralization using Amide I area (D) or Amide III area (E). D) A significant main effect of treatment was identified for relative mineralization using CH_2 wagging intensity, with both pre-existing and new bone that had received raloxifene showing a lower mineral-to-matrix ratio compared to untreated bone. For controls, treatment or matrix age had no significant impact on mineral crystallinity (F) or the Amide I mineral-to-matrix ratio (H). G) We observed a significant main effect of matrix age for relative type B carbonate substitution, with new bone displaying higher values than pre-existing bone. L) Raloxifene treatment resulted in a lower mineral-to-matrix ratio measuring CH_2 wagging and higher Amide III area (J) compared to untreated samples. Figure dipicts box and whisker plot; whiskers denote min. and max.

Quasi-static Nanoindentation

For CKD, we observed a significant main effect of matrix age for indentation modulus (p=0.02, **Fig.7A**) and hardness (p=0.04, **Fig.7B**) where values were lower in new bone versus pre-existing bone. Similarly, control bone demonstrated a main effect of matrix age for indentation modulus (p=0.007, **Fig.7C**) and hardness (p=0.01, **Fig.7D**) with lower values seen in the new bone. For all groups and matrix location, treatment with RAL trended toward an increase in modulus and hardness which failed to reach significance.

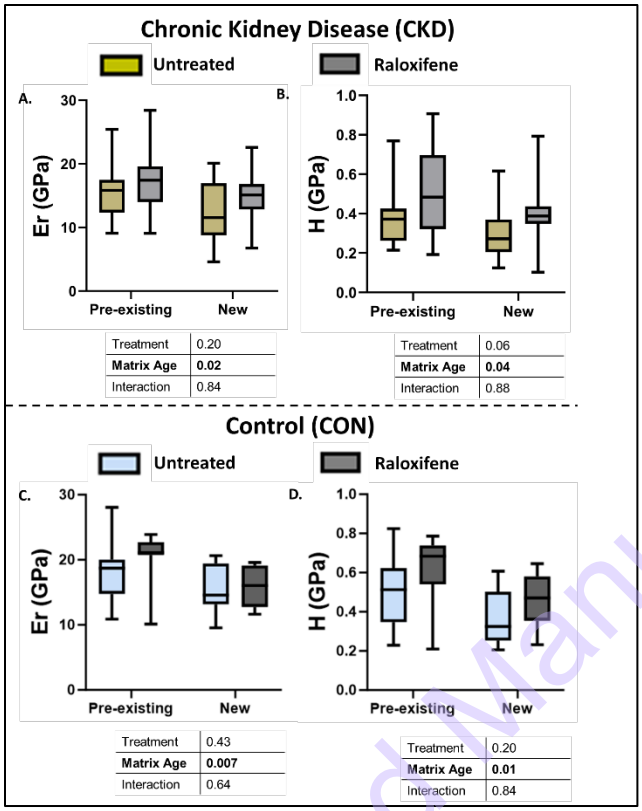

Figure 7. Quasi-static Nanoindentation. CKD tibiae had a significant main effect of matrix age for indentation modulus (A) and hardness (B) where measures were lower in the new bone versus pre-existing bone. Control bone also demonstrated a significant main effect of matrix age for modulus (C) and hardness (B) with new bone having lower values. Figure dipicts box and whisker plot; whiskers denote min. and max.

Dynamic Indentation Testing

In loaded CKD tibia, we observed a main effect of indentation depth for storage modulus (E', p=0.04), loss modulus (E'', p<0.0001), and tan delta (tanδ, P<0.0001) where E' increased and E'' and tanδ decreased as a function of increased testing depth (**Fig. 8A-C**). A main effect of indentation depth was seen for E'' (p=0.04) and tanδ (P<0.0001) for loaded control limbs where average E'' and tanδ decreased as a function of increased testing depth (**Fig. 8E-G**).

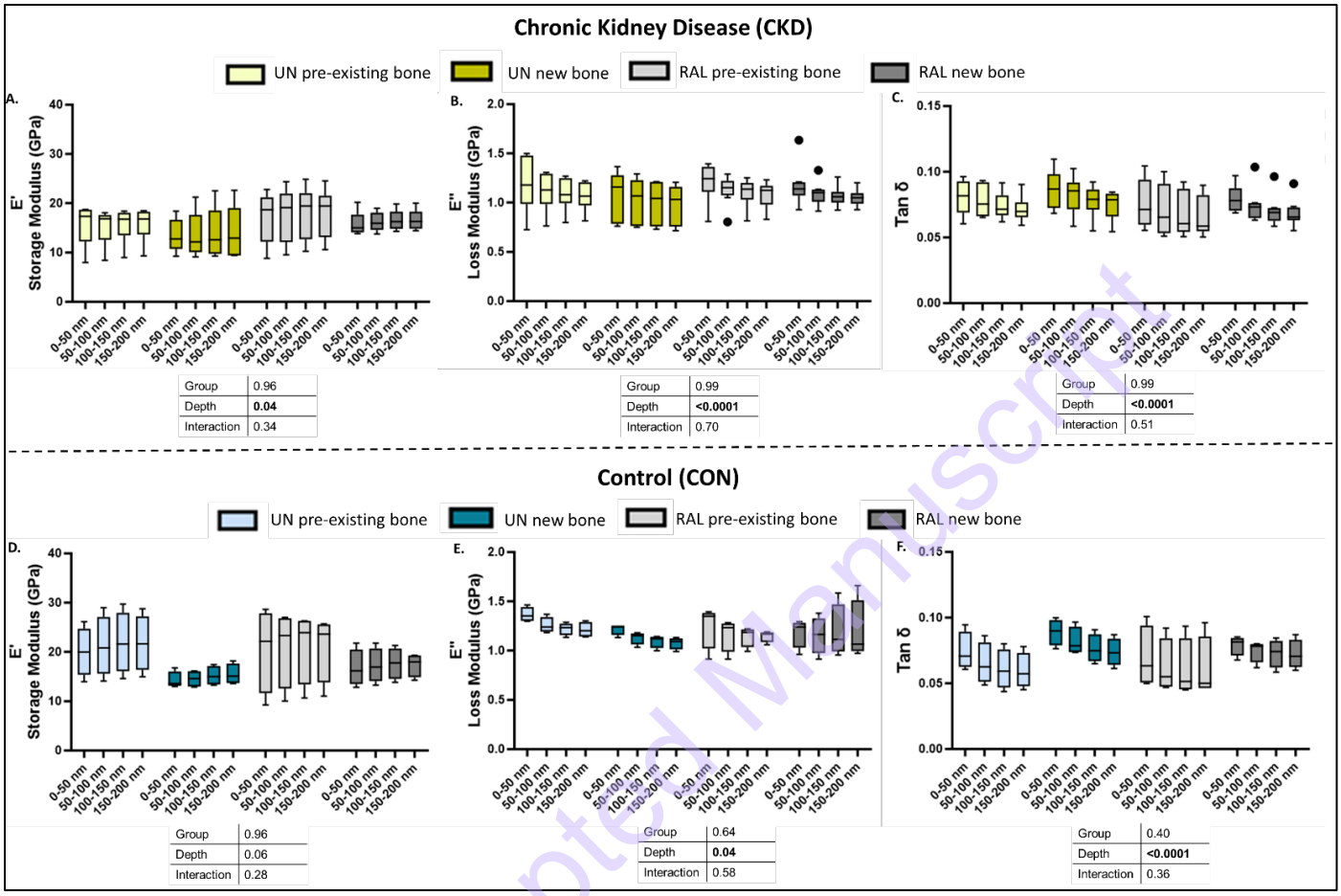

Figure 8. Dynamic indentation testing. Each indentation test used a constant strain rate CMX load function, oscillating the probe at 100 Hz and 5 µN dynamic load as the indenter was pushed into the bone until a 1000 µN peak static load was achieved. Thus, viscoelastic behavior was assessed as a function of indentation depth. In CKD, we observed a main effect of depth for storage modulus (A), loss modulus (B), and tanδ (C). Only loss modulus (E) and tanδ (F) but not storage modulus (D) were impacted by testing depth for control bone. Figure depicts box and whisker plot; whiskers denote min. and max.

Discussion

Multifaceted approaches that address cortical porosity and enhancing matrix composition are desired to normalize mechanical properties and improve skeletal health in CKD. This study aimed to assess the anabolic impact of in vivo mechanical loading, with and without adding raloxifene—a potential matrix-modifying therapeutic. Using the adenine-induced mouse model of CKD, we observed that mechanical loading reduced cortical porosity, improved several cortical geometry outcomes, and enhanced mechanical properties related to strength. The addition of raloxifene induced changes in cortical area, trabecular bone BV/TV, trabecular thickness, post-yield displacement, work, total strain, and toughness. The combination of loading and raloxifene further improved deformation and energy, resulting in even tougher, more ductile, and stronger bones. Furthermore, bones from animals treated with raloxifene had elevated matrix-bound water, a change significant only in the CKD cohort. Additionally, bound water was negatively associated with PTH levels, showing that animals with higher PTH levels often had the lowest bound water content. While control animals responded positively to loading, their bones were far less impacted by raloxifene treatment, showing no deformation, toughness, or bound water improvements. This multifaceted treatment was effective in generating new bone with reduced porosity (through loading) and improved matrix properties (with raloxifene), aiding in minimizing skeletal fragility induced by CKD.

We confirmed a steady-state CKD disease state was achieved prior to the initiation of treatment, where serum BUN and PTH were significantly elevated above control levels. A compromised CKD bone phenotype was also evident, characterized by increased cortical porosity, decreased trabecular number, and impaired whole bone mechanical and estimated material properties. Following 5 weeks of intervention, the CKD group maintained elevated BUN and PTH serum levels compared to the control group. Notably, the RAL-treated CKD group showed lower BUN (not significant), aligning with a trend observed in a previous study using the Cy/+ rat treated with RAL [23]. A post-hoc analysis of the MORE study—a randomized clinical trial using RAL in post-menopausal women with osteoporosis—showed that over three years, the RAL groups experienced slower increases in BUN and a slower decline in mean eGFR compared to the placebo group. This observation suggests potential renoprotective effects of RAL [36]. For body mass, the CKD mice unsurprisingly had lower body weight than controls which is well documented using the adenine chow-induced model. RAL treatment resulted in lower body weight than the UN group within each cohort (CKD, control). Previous work evaluating the RAL in male non-CKD rats observed that male body mass gain and food consumption were depressed at all dosage levels of RAL [37]. When assessing the kidney weight ratio, we observed that RAL treatment led to greater kidney mass compared to UN animals in both the control and CKD cohorts; however, histology was not conducted on the kidneys and thus the source of these changes were not elucidated.

Recent work has demonstrated that in animal models of progressive CKD, cortical porosity can infill through active bone formation [8]. We chose in vivo cyclic axial compressive loading to initiate bone formation in this study for several reasons: 1) in vivo loading is a robust anabolic stimulus in non-CKD models[9, 10], 2) repetitive mechanical loading using free wheel running has been shown to modify porosity and serum biochemistries in CKD models [11], and 3) in vivo loading of one limb leaves the contralateral limb as a non-loaded internal positive control, reducing the number of animals needed. In CKD animals, loading was responsible for a notably lower percent porosity of the tibia versus the non-loaded limb. While percent porosity was significantly lower, we cannot fully conclude that pores were infilled or if the loading intervention suppressed new pore formation throughout the 5 weeks. To evaluate this, repeated in vivo

µCT scans would need to be acquired longitudinally, registered across time points, and the pore dynamics quantified as we have shown in our previous work in humans using HRpQCT imaging[38, 39]. While loading-based exercise may be a viable intervention in some bone conditions, the effects of physical activity or exercise-based loading in CKD patients are less established, but resistance training is likely valuable[40]. Additional efforts are underway to identify therapeutics that can initiate bone formation, filling cortical pores through various methods of PTH suppression [41]. Finally, while mechanical intervention through cage wheel running in a CKD rat model demonstrated a decrease in PTH (which may have contributed to the concurrent lower porosity) in a study by Avin et al., we could not evaluate the impact of loading on serum biochemistries due to the study design where the right tibia of all mice were loaded[11]. Future work would need to implement a non-loaded CKD group to evaluate the impact of in vivo cyclic loading on serum PTH.

From a mechanical perspective, the effects of loading and RAL treatment were more robust in the CKD cohort. Mechanical loading primarily led to increased properties related to strength, such as yield and ultimate force. RAL, whether administered alone or in combination with loading, enhanced deformation, and energy, resulting in a bone that was tougher and more ductile, indicative of positive changes in the bone matrix. Loaded CKD limbs from untreated animals exhibited a higher elastic modulus compared to non-loaded limbs. Raloxifene treatment, however, "blunted" the stiffening effect from loading, resulting in bones with an overall similar modulus to non-loaded RAL-treated limbs and a lower modulus than untreated loaded limbs. Bone toughness was improved in CKD treated animals, consistent with previous observations. Interestingly, the property of toughness was not significantly impacted in the control cohort treated with RAL, nor were post-yield and total displacement, similar to what has been observed in previous work by members of our group suggesting that it may be difficult to make good bones better [42]. Despite similar impacts on cortical geometry in CKD and control measured by µCT, the greater improvements in mechanics in CKD suggest that additional changes beyond what can be detected in µCT are at play, including modulation of bone hydration and other compositional properties discussed in detail below.

We observed significantly higher matrix-bound water in the RAL-treated CKD cohort compared to UN CKD, nearly reaching levels observed in UN controls. Notably, bound water was not significantly higher in RAL-treated controls compared to UN controls. This observation supports findings from a prior ex vivo soaking study, where long bones from the adenine-fed CKD mouse model or control bone were exposed to a RAL solution for 14 days, and no significant change was observed in control bone exposed to RAL vs. vehicle solution[18]. While RAL treatment has demonstrated enhancement of matrix-bound water in other non-CKD animal models[20, 43], its positive impact was not evident when administered to the Cy/+ rat model of progressive CKD[23]. In Newman et al.'s study, improved skeletal properties, including enhanced mechanical toughness, were observed in Cy/+ rats treated with RAL. However, when bones were measured using ^{1}H NMR spectroscopy at 4.7T (without MAS), no significant difference in bound water by volume was observed due to treatment. The exact source of the disparity in observations remains unclear, but it could be attributed to variations in the method of determining bound water utilized across published studies.

Unsurprisingly, CKD cortical bone exhibited lower total and bound water than control cortical bone. This aligns with prior work in the Cy/+ model of progressive CKD, where animals with high turnover CKD (indicated by high PTH) demonstrated lower bound water levels compared to normal littermates[43]. Interestingly, the same study Cy/+ rats with low turnover CKD (low PTH) had higher bound water than their control littermates. This observation is noteworthy because, in our study, we observed a significant negative association between PTH and matrix-bound water; higher PTH levels corresponded to lower

bound water content. This is intriguing, given that the regulatory mechanism of bound water remains largely unknown. We speculate that there is likely some influence of PTH on bound water, whether directly through unknown signaling or because of a high-turnover state where the bone matrix (the location of bound water) is continually being resorbed. This aspect warrants further investigation. In a study by Rai et al., which utilized ssNMR to assess trabecular bone water in normal rats, those with bone loss, and those who received PTH following ovariectomy, it was observed that with bone restoration via PTH, bound water remained low even after an increase in bone mass[26]. This observation prompts further investigation into the PTH/bone water axis, supported by findings from Rai et al. indicating that, even after bone restoration via PTH, bound water remains low.

Interest in RAL's ability to modulate aspects of bone beyond the mineral was based on post-menopausal clinical studies with RAL that showed a significant decrease in fractures, not fully explained by a modest increase in BMD [44]. Preclinically, studies have shown RAL can increase bone water in an estrogen-independent manner by interacting with collagen and collagen/mineral interfaces[19, 20]. In CKD patients, the administration of RAL was associated with a significant increase in spine BMD and a reduction in vertebral fractures compared to placebo, regardless of kidney function, with a similar number of adverse events observed in both RAL and placebo-treated groups [45]. In another study, RAL-treated postmenopausal hemodialysis patients had reduced serum calcium levels [46]. It is essential to highlight that none of these clinical studies assessed bone quality metrics as an endpoint, leaving the impact of RAL on bone hydration and collagen in patients unknown. Evaluation of these metrics necessitates clinically relevant tools such as magnetic resonance imaging using ultrashort and zero echo time techniques (UTE-MRI), capable of measuring bone hydration and matrix organization in vivo [47].

In CKD, newly formed bone treated with RAL exhibited significantly higher mineral crystallinity, a measure which reflects mineral crystal size, shape, and perfection, compared to pre-existing bone similarly treated with RAL. Additionally, pre-existing RAL-treated mineral crystallinity was lower than in untreated pre-existing bone for CKD. These data suggest the development of new bone in preexisting tissue characterized by an abundance of smaller and less mature mineral crystals [48]. Lower crystallinity is associated with increased ductility (less brittleness), which could partly account for improvements observed in various 4-point bend testing parameters, including increased deformation/displacement once permanent damage has initiated in the matrix. When treated with RAL, CKD and control groups exhibited lower mineral-to-matrix ratios in both new and pre-existing tissues. The mineral-to-matrix ratio reflects the degree of mineralization in bone, suggesting that after five weeks of treatment, there was an increase in new bone formation with RAL that had not yet been fully mineralized. In both quasistatic nanoindentation and DMA, no main effect of treatment was evident for any outcome measure, although trends were observed. This is likely attributed to small sample sizes and high variability across the tested samples.

Limitations

There are several limitations to this study that are worth noting. First, the study exclusively utilized male mice, a choice driven in part by the study's scale, with plans to incorporate female mice in future experiments. Additionally, the study only captured endpoint outcomes, precluding the assessment of longitudinal changes resulting from the interventions, both in serum and outcomes such as porosity, where the evaluation of pore infilling would be particularly informative [41]. While ssNMR served as the method for bone hydration assessment in this study, UTE-MRI would offer a more clinically relevant

technique. However, practical constraints, including the size of mouse bones and the achievable resolution using MRI, limited our choice. Subsequent studies aiming to evaluate bone water preclinically may find employing rats (with larger bone size) necessary if UTE-MRI is a primary outcome. In our examination of nano DMA, we investigated viscoelastic properties with depth as a variable. However, a more suitable approach would involve assessing these properties in relation to a varying frequency at a constant depth. This approach would assess the material's response to varying loading rates, as opposed to assessing a property gradient as a function of indentation depth (which we would not anticipate given the method of treatment). Subsequent work in our laboratory is planning to focus on this approach. The study faced limitations in terms of the number of bones utilized for material-level mechanical property assessments (nanoindentation) and Raman spectroscopy.

Conclusions

Addressing cortical porosity induced by CKD is crucial, but it is likely insufficient for maximizing the enhancement of mechanical properties. Thus, an effective treatment program to improve fracture risk in CKD likely requires focusing both cortical porosity and matrix properties. Our data suggest that administering a bone hydration-modifying treatment, such as raloxifene, can improve bone matrix properties in newly formed bone which often exists in high turnover CKD. Bones from animals that received both in vivo loading and raloxifene had lower porosity and higher matrix-bound water and could undergo a greater amount of deformation before failing.

Declaration of Competing Interests

The authors have no competing interests to disclose.

Acknowledgments

This work was supported by the National Science Foundation [LEAP-HI 1952993 (RKS, MRA, JMW], the National Institutes of Health [LRP 1L30DK130133-0 (RKS), R01AR072609 (JMW)], T32 AR065971 (AAT), and the United States (U.S.) Department of Veterans Affairs Merit Grant (BX003025 and IK6BX006479, MRA). The content is solely the responsibility of the authors and does not necessarily represent the official views of the National Science Foundation, the National Institutes of Health or the VA.

References

1. Mittalhenkle, A, et al., *Increased risk of mortality associated with hip fracture in the dialysis population.* Am J Kidney Dis, 2004. **44**(4): p. 672-9.
2. Coco, M, et al., *Increased incidence of hip fractures in dialysis patients with low serum parathyroid hormone.* Am J Kidney Dis, 2000. **36**(6): p. 1115-21.
3. Burr, DB, *Cortical bone: a target for fracture prevention?* Lancet, 2010. **375**(9727): p. 1672-3.
4. Seeman, E, *Overview of bone microstructure, and treatment of bone fragility in chronic kidney disease.* Nephrology (Carlton), 2017. **22 Suppl 2**: p. 34-35.
5. Nickolas, TL, et al., *Bone mass and microarchitecture in CKD patients with fracture.* J Am Soc Nephrol, 2010. **21**(8): p. 1371-80.
6. Hasegawa, T, et al., *Evocalcet Rescues Secondary Hyperparathyroidism-driven Cortical Porosity in CKD Male Rats.* Endocrinology, 2023. **164**(4).
7. Surowiec, RK, et al., *Tracking changes of individual cortical pores over 1 year via HR-pQCT in a small cohort of 60-year-old females.* Bone Rep, 2022. **17**: p. 101633.
8. Metzger, CE, et al., *Reversing cortical porosity: Cortical pore infilling in preclinical models of chronic kidney disease.* Bone, 2020: p. 115632.
9. Berman, AG, et al., *Structural and Mechanical Improvements to Bone Are Strain Dependent with Axial Compression of the Tibia in Female C57BL/6 Mice.* PLoS One, 2015. **10**(6): p. e0130504.
10. Weatherholt, AM, et al., *Cortical and trabecular bone adaptation to incremental load magnitudes using the mouse tibial axial compression loading model.* Bone, 2013. **52**(1): p. 372-9.
11. Avin, KG, et al., *Voluntary Wheel Running Has Beneficial Effects in a Rat Model of CKD-Mineral Bone Disorder (CKD-MBD).* J Am Soc Nephrol, 2019. **30**(10): p. 1898-1909.
12. Newman, CL, et al., *Cortical bone mechanical properties are altered in an animal model of progressive chronic kidney disease.* PLoS One, 2014. **9**(6): p. e99262.
13. Iwasaki, Y, et al., *Altered material properties are responsible for bone fragility in rats with chronic kidney injury.* Bone, 2015. **81**: p. 247-254.
14. Nyman, JS, et al., *Measurements of mobile and bound water by nuclear magnetic resonance correlate with mechanical properties of bone.* Bone, 2008. **42**(1): p. 193-9.
15. Willett, TL, et al., *Bone collagen network integrity and transverse fracture toughness of human cortical bone.* Bone, 2019. **120**: p. 187-193.
16. Wang, X, et al., *Age-Related Deterioration of Bone Toughness Is Related to Diminishing Amount of Matrix Glycosaminoglycans (Gags).* JBMR Plus, 2018. **2**(3): p. 164-173.
17. Rajapakse, CS, et al., *Volumetric Cortical Bone Porosity Assessment with MR Imaging: Validation and Clinical Feasibility.* Radiology, 2015. **276**(2): p. 526-35.
18. Surowiec, RK, et al., *Ex vivo exposure to calcitonin or raloxifene improves mechanical properties of diseased bone through non-cell mediated mechanisms.* Bone, 2023. **173**: p. 116805.
19. Bivi, N, et al., *Structural features underlying raloxifene's biophysical interaction with bone matrix.* Bioorg Med Chem, 2016. **24**(4): p. 759-67.
20. Gallant, MA, et al., *Bone cell-independent benefits of raloxifene on the skeleton: a novel mechanism for improving bone material properties.* Bone, 2014. **61**: p. 191-200.
21. Berman, AG, et al., *Raloxifene reduces skeletal fractures in an animal model of osteogenesis imperfecta.* Matrix Biol, 2016. **52-54**: p. 19-28.
22. Allen, MR, et al., *In Vivo UTE-MRI Reveals Positive Effects of Raloxifene on Skeletal-Bound Water in Skeletally Mature Beagle Dogs.* J Bone Miner Res, 2015. **30**(8): p. 1441-4.
23. Newman, CL, et al., *Raloxifene improves skeletal properties in an animal model of cystic chronic kidney disease.* Kidney Int, 2016. **89**(1): p. 95-104.

24. Metzger, CE, et al., *Elevations in Cortical Porosity Occur Prior to Significant Rise in Serum Parathyroid Hormone in Young Female Mice with Adenine-Induced CKD.* Calcif Tissue Int, 2020. **106**(4): p. 392-400.
25. Wallace, JM, et al., *Inbred strain-specific response to biglycan deficiency in the cortical bone of C57BL6/129 and C3H/He mice.* J Bone Miner Res, 2009. **24**(6): p. 1002-12.
26. Rai, RK, et al., *Total water, phosphorus relaxation and inter-atomic organic to inorganic interface are new determinants of trabecular bone integrity.* PLoS One, 2013. **8**(12): p. e83478.
27. van Rossum, B-J, et al., *High-Field and High-Speed CP-MAS ¹³C NMR Heteronuclear Dipolar-Correlation Spectroscopy of Solids with Frequency-Switched Lee-Goldburg Homonuclear Decoupling.* Journal of Magnetic Resonance, 1997. **124**: p. 516-519.
28. Fung, BM, et al., *An improved broadband decoupling sequence for liquid crystals and solids.* J Magn Reson, 2000. **142**(1): p. 97-101.
29. Levitt, MH, et al., *High-resolution 1H NMR in solids with frequency-switched multiple-pulse sequences.* Solid State Nucl Magn Reson, 1993. **2**(4): p. 151-63.
30. Dwivedi, N, et al., *Unraveling Water-Mediated (31)P Relaxation in Bone Mineral.* ACS Omega, 2022. **7**(19): p. 16678-16688.
31. Kaflak, A, et al., *Phosphorus-31 spin-lattice NMR relaxation in bone apatite and its mineral standards.* Solid State Nucl Magn Reson, 2007. **31**(4): p. 174-83.
32. Pines, A, et al., *Proton-enhanced NMR of dilute spins in solids.* The Journal of chemical physics, 1973. **59**(2): p. 569-590.
33. Zhu, P, et al., *Time-resolved dehydration-induced structural changes in an intact bovine cortical bone revealed by solid-state NMR spectroscopy.* J Am Chem Soc, 2009. **131**(47): p. 17064-5.
34. Damrath, JG, et al., *Calcimimetics Alter Periosteal and Perilacunar Bone Matrix Composition and Material Properties in Early Chronic Kidney Disease.* J Bone Miner Res, 2022. **37**(7): p. 1297-1306.
35. Oliver, WC, et al., *An improved technique for determining hardness and elastic modulus using load and displacement sensing indentation experiments.* Journal of Materials Research, 1992. **7**(6): p. 1564-1583.
36. Melamed, ML, et al., *Raloxifene, a selective estrogen receptor modulator, is renoprotective: a post-hoc analysis.* Kidney International, 2011. **79**(2): p. 241-249.
37. Hoyt, JA, et al., *The Selective Estrogen Receptor Modulator, Raloxifene: Reproductive Assessments in Adult Male Rats 11These studies were conducted in accordance with the Food and Drug Administration "Good Laboratory Practice Regulations for Nonclinical Laboratory Studies." CRF Part 58, 1978.* Reproductive Toxicology, 1998. **12**(3): p. 223-232.
38. Surowiec, RK, et al., *Bone hydration: How we can evaluate it, what can it tell us, and is it an effective therapeutic target?* Bone Rep, 2022. **16**: p. 101161.
39. Swallow, EA, et al., *Cortical porosity development and progression is mitigated after etelcalcetide treatment in an animal model of chronic kidney disease.* Bone, 2022. **157**: p. 116340.
40. Cardoso, DF, et al., *Impact of physical activity and exercise on bone health in patients with chronic kidney disease: a systematic review of observational and experimental studies.* BMC Nephrology, 2020. **21**(1): p. 334.
41. Metzger, CE, et al., *Reversing cortical porosity: Cortical pore infilling in preclinical models of chronic kidney disease.* Bone, 2021. **143**: p. 115632.
42. Berman, AG, et al., *Effects of Raloxifene and tibial loading on bone mass and mechanics in male and female mice.* Connect Tissue Res, 2022. **63**(1): p. 3-15.
43. Allen, MR, et al., *Changes in skeletal collagen cross-links and matrix hydration in high- and low-turnover chronic kidney disease.* Osteoporos Int, 2015. **26**(3): p. 977-85.

44. Riggs, BL, et al., *Bone Turnover Matters: The Raloxifene Treatment Paradox of Dramatic Decreases in Vertebral Fractures Without Commensurate Increases in Bone Density.* Journal of Bone and Mineral Research, 2002. **17**(1): p. 11-14.
45. Ishani, A, et al., *The effect of raloxifene treatment in postmenopausal women with CKD.* J Am Soc Nephrol, 2008. **19**(7): p. 1430-8.
46. Tanaka, M, et al., *Effects of Raloxifene on Bone Mineral Metabolism in Postmenopausal Japanese Women on Hemodialysis.* Therapeutic Apheresis and Dialysis, 2011. **15**(s1): p. 62-66.
47. Ma, Y-J, et al., *Quantitative Ultrashort Echo Time (UTE) Magnetic Resonance Imaging of Bone: An Update.* Frontiers in Endocrinology, 2020. **11**.
48. Gamsjaeger, S, et al., *Bone material properties in actively bone-forming trabeculae in postmenopausal women with osteoporosis after three years of treatment with once-yearly Zoledronic acid.* J Bone Miner Res, 2011. **26**(1): p. 12-8.